Uppsala 1968

LENNART BÄCKERUD

Kinetic aspects of the solidification of binary and ternary alloy systems

Preprint from

Jernkontorets Annaler vol. 152, 1968 pp. 109–138

Digitized by the Internet Archive
in 2026

https://archive.org/details/IA41548909_0034

KINETIC ASPECTS OF THE SOLIDIFICATION OF BINARY AND TERNARY ALLOY SYSTEMS

L. Bäckerud

536.421.4:669.715'1'74

INTRODUCTION

Our present knowledge of metallic systems is essentially based on the work which chemists, crystallographers and metallurgists have carried out to study equilibrium reactions, to solve structural problems, to study the range of existence for intermetallic compounds and so on. Thermodynamic aspects of phase formation and growth processes have often been successfully applied. One of the main difficulties which we encounter is the sluggishness by which these systems attain equilibrium.

Especially concerning solidification processes, kinetic aspects of phase formation and growth processes have often been overlooked. In many industrial processes, the element and phase distribution in castings is often very different from the equilibrium conditions. These deviations will be especially marked at fast solidification processes, which due to progress in continuous casting technique have been more and more common.

In the present work the element distribution and phase formation in the systems Al-Fe, Al-Mn and Al-Mn-Fe have been studied. The interest has been limited to aluminium-rich alloys (Al > 95%), which are of technical importance.

The principle observations made concerning the deviation of these alloy-systems from the equilibrium reactions, however, must not be considered as limited only to these types of alloys, but be assumed to have parallels within many other metallic systems.

Fundamental concepts concerning solidification processes have been clarified by Prof. Bruce Chalmers in his book "Principles of Solidification".

SOME KINETIC ASPECTS OF PHASE FORMATION AND GROWTH IN ALUMINIUM-IRON ALLOYS

Literature review

A general survey over the constitution of the Al-Fe system can be found in the reference works by Hansen [1] and Elliott [2].

An extensive treatment of the knowledge gathered up to 1965 about Al-Fe alloys and their properties has been made by Altenpohl [3].

The generally accepted equilibrium phase diagram is based on measurements by Roth [4], Edgar [5], Crussard and Aubertin [6], and others.

As seen from Fig. 1 a eutectic reaction takes place at 655°C at an Fe content of about 1.7 weight percent. At this temperature the α-phase has its maximum solubility, which is reported to be 0.052% Fe. In equilibrium with the α-phase stays a binary Al-Fe-intermetallic compound, which is denoted Al_3Fe. The constitution of this intermetallic compound has been discussed at length (e.g. by Raynor and Pfeil [7], Bradley and Taylor [8] and Black [9]), but in this work no detailed study over the range of existence of the phase or its constitution has been made. The phase will be denoted Al_3Fe and will be considered as a monoclinic crystal in accordance with the statements made by Black [9].

In 1962 Hollingsworth *et al.* [10] reported that a new Al-Fe intermetallic compound had been discovered in rapidly chilled ingots of the composition Al + 2% Fe. This phase gave x-ray diffraction patterns very similar to the well-known compound Al_6Mn, and it was assumed to have the composition Al_6Fe. A crystal of this type was isolated and studied in detail by Walford [11], who confirmed that the new phase is isostructural with the corresponding Al-Mn compound. Altenpohl [3] assumes that the phase Al_6Fe most probably is to be found in material of commercial purity, which has been produced by a strip casting technique, where the rate of heat transfer is very high.

In accordance with the definition of equilibrium condition, which in a general form has been given by Chalmers [12] and later discussed by Bäckerud and Chalmers [13], kinetic aspects of the solidification process must be taken into consideration in the determination of a "true" equilibrium diagram.

No theories have been proposed to predict quantitatively the composition of the first growing solid

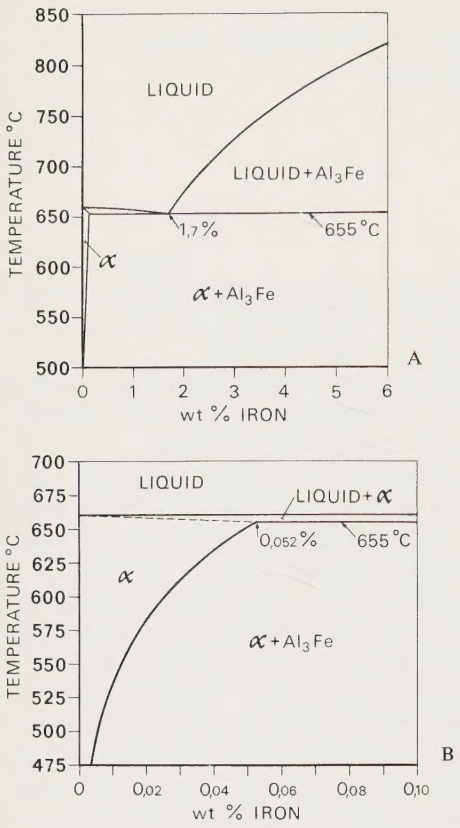

Fig. 1. Parts of the aluminium-iron equilibrium phase diagram. A) according to Phillips [35], B) according to Edgar [5].

phase in a binary system, similar to the Al-Fe system, when the alloy content of the melt is far above the maximum solid solubility of the alloying component. As a comparison to this problem it can be mentioned that after Rutter and Chalmers [14] in 1953 had defined the concept of "constitutional supercooling", Tiller *et al.* [15] theoretically derived and experimentally verified an expression for determining the composition of a growing crystal with a planar surface and of the solute enrichment ahead of this surface. However, the prediction assumed that the initial composition of the melt was below the solid solubility for the alloying element in question. Furthermore there were limitations in the theory concerning temperature gradients and growth rates.

Bäckerud and Chalmers [13] have described a method for determining a "true" equilibrium diagram from cooling curves, taking kinetic aspects into consideration. The method is applicable also when the phases grow dendritically. They worked with a binary system with a relatively large partition ratio and a high solid solubility of the alloying element (Al-Cu). In the system Al-Fe which is characterized by an extremely small partition ratio and a very low solid solubility of iron in solid aluminium, the actual growth temperature of the α-phase will be far below the liquidus temperature found from the equilibrium phase diagram. The actual distribution of elements and phases in cases like these can be described in dynamic phase diagrams, each one valid only for a particular rate of freezing. By extrapolating points on these dynamic diagrams back to the growth rate zero, the "true" equilibrium phase diagram can be established.

A critical examination of published data about the composition and temperature for the eutectic reaction in the Al-Fe system shows that the given eutectic points are scattered over a considerable area in the phase diagram (see Fig. 2).

This scatter of the points may not only depend on lack of accuracy in the measuring technique, or, as Hansen [1] states, on impurities in the base material, but may be a result of the fact that kinetic factors influencing the solidification process have not been considered enough.

In the following section the results of carefully determined cooling curves, metallographic and physical investigations of samples produced under varying conditions of solidification with different composition within the aluminium-rich part of the Al-Fe system will be shown. By evaluating these experiments it will be possible to clarify nucleation and growth processes and to determine the conditions for transformations between different possible intermetallic phases.

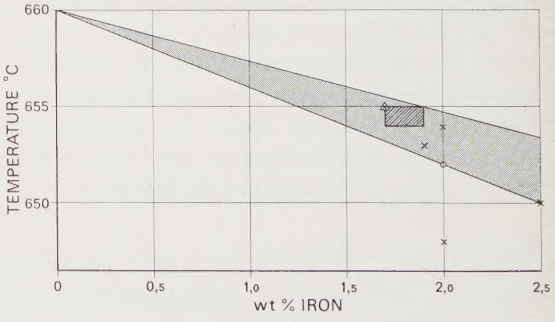

Fig. 2. The composition and temperature of the Al-Al_3Fe eutectic according to different sources.
△ Recommendation by Altenpohl [3].
▨ Recommendation by Hansen [1].
× Measurements referred to by Hansen [1].
○ Recommendation by Lee [36].

Growth of the α-phase

The temperature at which the first solid phase (the dendritic network) forms in a melt depends on constitutional factors which are described in the phase diagram, but also on the rate at which heat is dissipated from the system and thereby the rate of growth (kinetic effects).

Bäckerud [16] has experimentally determined the following relationship:

$$(\Delta T)^2 = A\frac{(1-k)(dQ/d\tau)}{k} \qquad (1)$$

where ΔT is the degree of undercooling relative to the "true" equilibrium diagram, at which the dendritic network grows, A is a constant, k is the partition ratio for the alloy system in question, and $dQ/d\tau$ is the rate at which heat is dissipated, e.g. measured as calories per second.

As the partition ratio in the Al-Fe system is exceptionally low ($k \approx 0{,}03$), the factor $(1-k)/k$, which is an expression for the degree of constitutional undercooling, is large.

It should be mentioned here that even low iron concentrations in the Al-Fe system cause a cellular growth mechanism of the α-phase in all normal industrial casting processes. This is easily seen if technical data are inserted in the equation which gives the limit for growth of a planar surface.

$$\frac{G}{R} \geq \frac{m C_0}{D} \cdot \frac{(1-k)}{k} \qquad (2)$$

where G is the temperature gradient in the melt, R is the rate of growth, m is the slope of the liquidus line in the equilibrium phase diagram, C_0 is the average concentration of solute in the melt, and D is the diffusion constant of the solute element in the liquid phase.

This equation was first derived by Tiller, Jackson, Rutter and Chalmers [15].

The conditions necessary to maintain a planar surface according to eq. (2) will never be fulfilled in normal technical processes, and even from iron concentrations of about 0.01 % a cellular-dendritic mode of growth is always expected.

The low partition ratio in the Al-Fe system causes a very high solute build-up in front of and between the growing dendrites. That part of the total undercooling ΔT which is caused by this solute build-up effect will here be called $\Delta T_{S(olute)}$.

At increasing rates of growth, the radii of the growing dendritic tips will be smaller and smaller, and due to surface tension effects the degree of undercooling relative to the liquidus temperature given by the equilibrium phase diagram will increase. The result of this effect will be designated $\Delta T_{R(adius)}$.

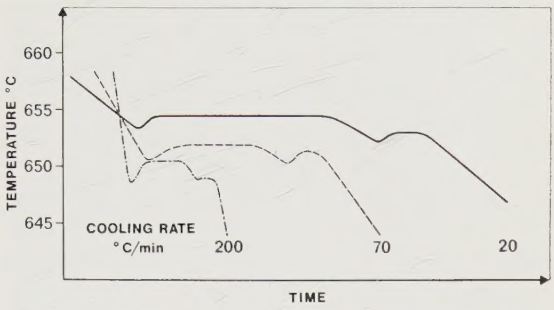

Fig. 3. Cooling curves from aluminium samples with 1% iron, measured at different rates of heat transfer.

A certain degree of undercooling is necessary to produce the net driving force for the atoms in the liquid to attach themselves to the growing solid. This kinetic growth function is designated $\Delta T_{K(inetic)}$.

Thus $\Delta T = \Delta T_S + \Delta T_R + \Delta T_K$

ΔT has been measured for different compositions in the Al-Fe system as a function of the rate of heat transfer.

In cylindrical graphite moulds, samples with a weight of around 75 g have been allowed to solidify at different rates, and the temperature in the centre of

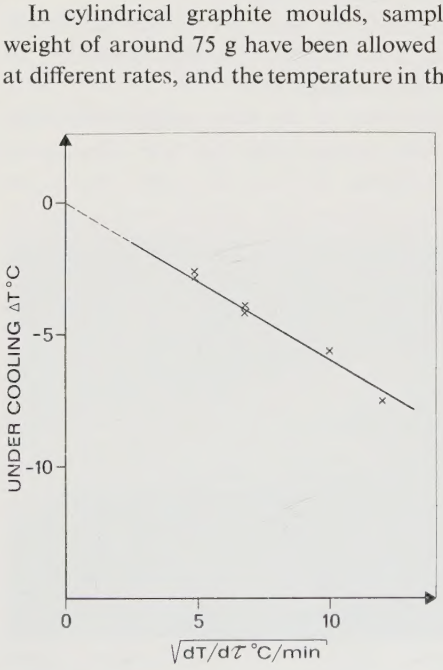

Fig. 4. The measured degree of undercooling (ΔT) as a function of cooling rate in aluminium samples with 1 % iron.

×100

Fig. 5. Microstructure of an aluminium sample with 1% iron, produced at a cooling rate of 20°C/min, showing the intermetallic phase Al_3Fe. Unetched.

×100

Fig. 7. Microstructure of an aluminium sample with 1% iron, produced at a cooling rate of 600°C/min, showing Al-Al_6Fe eutectic areas. Unetched.

the sample has been recorded during the solidification process. In order to get high accuracy in the temperature recording the difference in EMF between the thermocouple in the sample and a reference couple kept at a constant temperature has been fed into a recorder with a sensitivity of 1 mV for full scale deflection. Temperature variations within 0.1°C will be read without difficulty. The technique has been described in reference [13]. Some typical cooling curves are shown in Fig. 3.

It is obvious from these curves that the actual growth rate of the α-phase is heavily dependent on the rate of heat transfer.

The significance of the long temperature-arrest plateau in the cooling curves has been discussed at length in reference [13]. In the same way as described in this reference, the arrest temperatures, which have to be identified with the actual temperature of growth of the α-phase, have been plotted against the rate of heat transfer in Fig. 4. In this diagram it can be seen that a cooling rate as low as 1°C/min gives an undercooling to the growing α-phase, relative to the "true" equilibrium diagram, which equals 0.6°C. Thus even small variations in the rate of the heat transfer lead to pronounced deviations from the state of equilibrium.

From curves similar to those in Fig. 4, measured at different concentrations in the Al-Fe system, it is possible to draw a "true" equilibrium liquidus curve by extrapolating the measured points back to zero speed of growth.

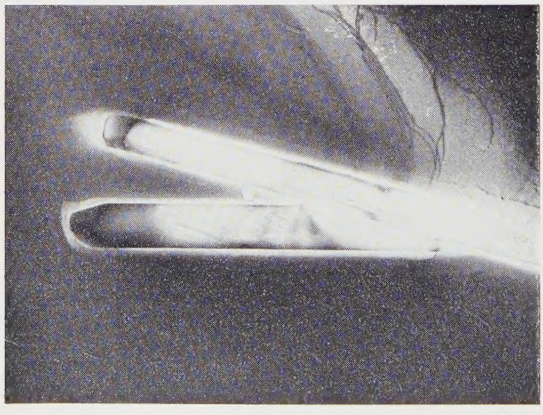

×20,000

Fig. 6. Details of Al_3Fe-crystals. Electron transmission microscopy.

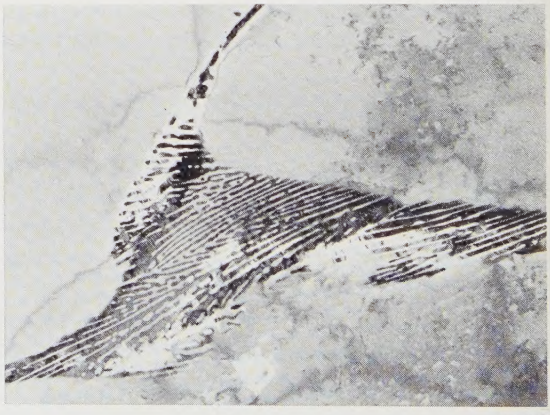

×2 000

Fig. 8. Details of Al-Al_6Fe eutectic. Electron transmission microscopy.

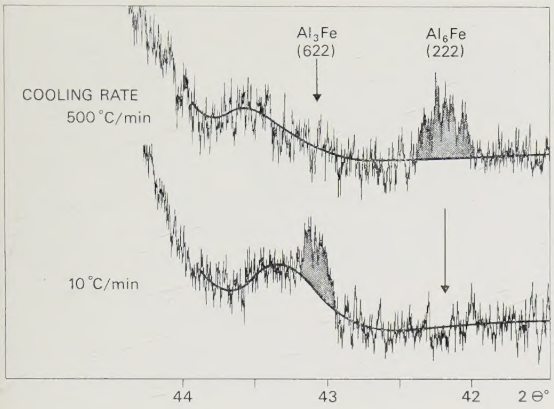

Fig. 9. Parts of x-ray diffractograms showing the presence of Al_3Fe at low, and of Al_6Fe at high cooling rates.

×100

Fig. 10. Microstructure of an aluminium sample with 1% iron, produced at a cooling rate of 60°C/min, showing Al-Al_3Fe eutectic areas. Unetched.

Intermetallic compounds in the Al-Fe system

Formation in hypo-eutectic alloys. Cooling curves similar to those in Fig. 3 show that eutectic growth takes place within two distinct temperature ranges. At slow solidification processes (<200°C/min), a eutectic grows between 650 and 655°C. (Also this temperature is of course dependent on the rate of heat transfer.) The growth of this eutectic phase starts only after a marked degree of undercooling, which indicates that the second phase in the eutectic is difficult to nucleate. At high rates of heat transfer another eutectic is formed, below 650°C, and apparently this phase has no difficulty to nucleate.

A metallographic examination of a number of samples from melts with 0.5–1% Fe, obtained at different rates of cooling, shows that samples which were solidified slowly contain well developed needle-shaped crystals of a type which is characteristic for the phase Al_3Fe. See Figs. 5 and 6. X-ray diffraction patterns obtained from the particles in situ verify the presence of the phase Al_3Fe.

X-ray diffraction analysis of the lamellar eutectic, which forms at high cooling rates, clearly indicates the presence of the phase Al_6Fe. The microstructure in this latter case is shown in Figs. 7 and 8. Parts of the x-ray diffractograms, showing the diffraction peaks (622) in Al_3Fe and (222) in Al_6Fe, are reproduced in Fig. 9.

The transition between the two different eutectic reactions seems to take place completely at a cooling rate around 200°C/min. Only occasionally have both phases been identified in one and the same sample. (In large castings and ingots, where the solidification rate varies from the surface and inwards, both types of eutectic can naturally be found.)

The four figures 5, 10, 11 and 7 show how the structure is changed with increasing cooling rate in hypo-eutectic Al-Fe alloys. All samples shown contain 1% Fe, and the cooling rates in these samples were 20, 60, 150 and 600°C/min, respectively.

Before the phase formation from hyper-eutectic alloys is discussed, a series of four pictures illustrate how the microstructure is changing with the composition. The samples shown in Figs. 12, 10, 13 and 14 contain 0.5, 1.0, 2.0 and 4.0% Fe, respectively, and have all been solidified at the same cooling rate of 60°C/min.

×100

Fig. 11. Microstructure of an aluminium sample with 1% iron, produced at a cooling rate of 150°C/min, showing both Al-Al_3Fe and Al-Al_6Fe eutectic areas. Unetched.

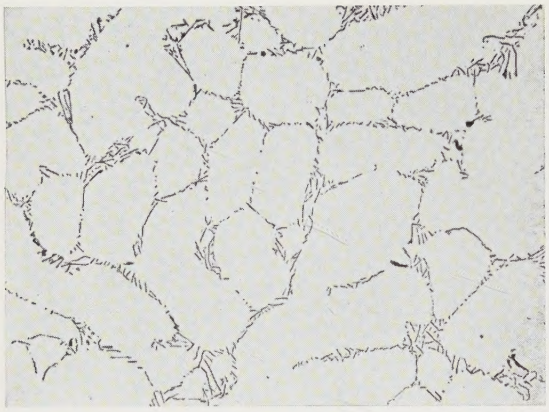

×100

Fig. 12. 0.5% iron.

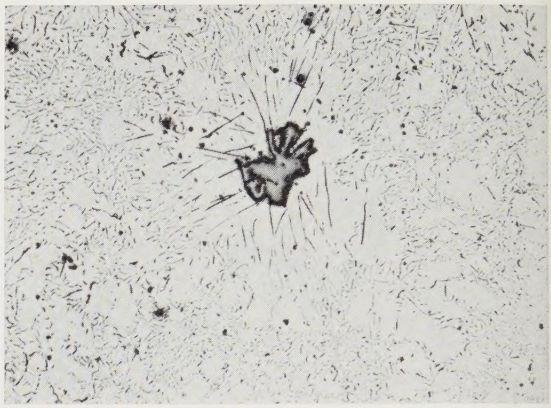

×100

Fig. 14. 4% iron.

Fig. 12–14. Microstructure of aluminium samples with varying iron contents, produced at a cooling rate of 60°C/min. Unetched.

Formation in hyper-eutectic alloys. The actual growth temperature of the α-phase as well as of eutectics is dependent on the rate of heat extraction from the solidifying material. The composition and temperature at which a eutectic reaction takes place will therefore vary with the cooling rate. To study further the formation and growth of phases in the Al-Fe system, a number of samples containing 2–4% Fe were produced at different cooling rates. These samples all had a composition which, according to published equilibrium phase diagrams, should be defined as hyper-eutectic.

The microstructures of two such samples with 2 and 4% Fe, both solidified at a cooling rate of 60°C/min, are shown in Figs. 13 and 14. The cooling curve taken from the former of these samples is shown in Fig. 15. At this cooling rate (60°C/min) the only intermetallic compound, which could be identified by x-ray diffraction was the Al_3Fe phase. The α-phase exhibits a typical dendritic mode of growth, as can be seen from Fig. 13. The cooling curve in Fig. 15 shows that there is a pronounced undercooling before the nucleation of a solid phase.

It is very probable that both the α-phase and the Al_3Fe phase nucleate simultaneously and start a eutectic growth. That means that the two phases develop a coupled growth pattern.

The α-phase, however, can grow faster than the Al_3Fe phase by developing a dendritic mode of growth. (This phenomenon will be discussed in detail in the following section.) At high rates of heat transfer, therefore, the α-phase will grow preferentially and the iron content of the remaining melt will concentrate in interdendritic areas, until finally the development of a "true, dynamic" eutectic will

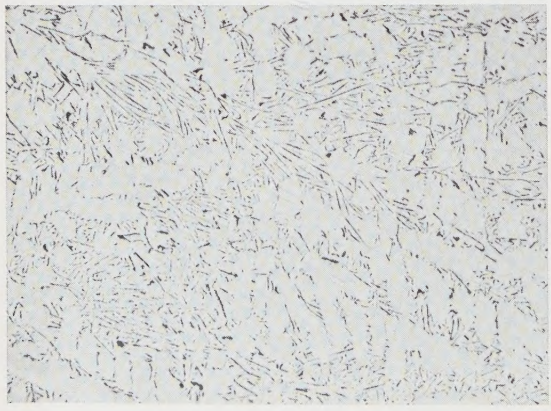

×100

Fig. 13. 2% iron.

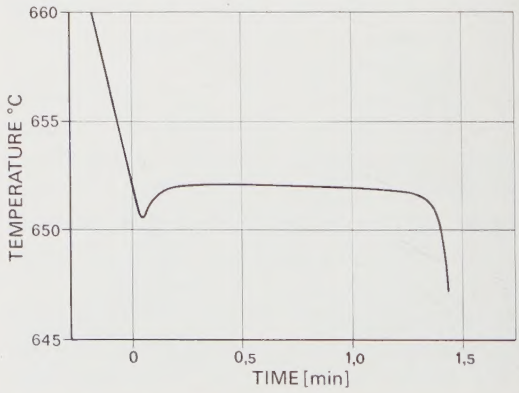

Fig. 15. Cooling curve taken from an aluminium sample with 2% iron, at a cooling rate of 60°C/min.

be the thermodynamically most favourable reaction to occur.

At very high rates of heat transfer the original supercooling will be high enough to favour the nucleation and growth of the Al-Al_6Fe eutectic.

When samples with 4% Fe are solidified, the Al_3Fe phase seems to be the primary phase to nucleate and to grow at all cooling rates studied (from 20 to 600°C/min). This can be observed from cooling curves and micrographs.

The microstructure of a sample, cooled at 60°C/min, is shown in Fig. 14 and the corresponding cooling curve in Fig. 16. The micrograph shows a primary Al_3Fe particle and its nearest surroundings. In the immediate vicinity of the Al_3Fe particle the melt seems to have been depleted of iron, and between some needle-shaped Al_3Fe particles a large area of α-phase has been formed. In the remaining melt there has been a competition in growth rate between the two different types of phases present and, in the same way as described above for the sample with 2% Fe, the α-phase grows preferentially in a dendritic manner. Finally, in the interdendritic areas, a true eutectic growth takes place. These different stages of the solidification process are discernible in the cooling curve. In samples with 4% Fe, the Al_6Fe phase has not been found in the very rapidly chilled samples.

Discussion on formation and growth of phases in the Al-Fe system

It has been shown in the preceding paragraphs that two different eutectic reactions occur in the Al-Fe system. The normal Al-Al_3Fe eutectic forms at temperatures above 650°C, and below this temperature the metastable eutectic reaction giving rise to Al-Al_6Fe takes place.

The factor controlling these reactions is the rate of heat transfer, in this work expressed as $dT/d\tau$ (°C/min). For a given size and geometry of sample and mould this expression can easily be converted into heat units per time unit, e.g. cal/s.

The Al_3Fe phase is obviously difficult to nucleate, and the melt of nearly eutectic composition therefore easily undercools. The Al-Al_3Fe eutectic reaction will take place only if the period of time, during which melt of the proper composition passes from the growth temperature of the α-phase (which is obtainable from Fig. 4) down to 650°C, is long enough to give high nucleation probability of the Al_3Fe phase.

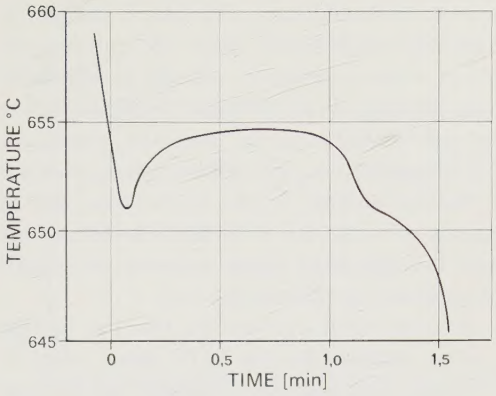

Fig. 16. Cooling curve taken from an aluminium sample with 4% iron, at a cooling rate of 60°C/min.

On the other hand, if the rate of heat transfer is high, the eutectic melt will be undercooled below 650°C before a noticeable number of Al_3Fe nuclei have been formed. At this lower temperature, the growth of the Al_6Fe phase is thermodynamically favoured. The degree of undercooling before the start of growth of this phase is always very low, which indicates that this phase nucleates easier than the Al_3Fe phase.

In Fig. 17 the temperature at which the eutectic reactions start has been plotted against the rate of heat transfer in the region near the transition point. The two lines intersect at 650°C and at a rate of heat transfer corresponding to 190°C/min.

As was described earlier, samples of hyper-eutectic composition (≈4% Fe) usually undercool to temperatures between 650 and 652°C before the nucleation of Al_3Fe particles, which in that type of alloy grow as the primary phase.

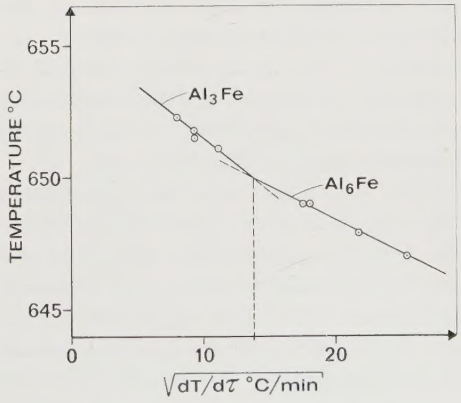

Fig. 17. The temperature at which eutectic reactions are initiated in samples of aluminium with 1% iron as a function of cooling rate.

The same undercooling is obtained in samples of hypo-eutectic composition, where the particles are formed in volume elements enclosed in the interdendritic spacings. As no difference in the nucleation temperature of Al_3Fe can be measured whether α-phase is present or not, the α-phase can be ruled out as an effective nucleant for the Al_3Fe phase, and as homogeneous nucleation is unlikely to occur, this indicates that the Al_3Fe phase nucleates on impurities or dispersed particles in the melt.

On the other hand it is possible that the α-phase is an active nucleant for the Al_6Fe phase, which is orthorhombic and with low disregistry can be fitted to the α-crystals. This hypothesis could explain the very low degree of undercooling necessary to start nucleation of the Al_6Fe phase.

The two eutectics formed in the Al-Fe system exhibit different growth habits. Hunt and Jackson [17] have studied eutectics and related their morphology to the growth mechanism of the participating phases.

The basic ideas of growth mechanisms leading to the classification of eutectics were presented by Jackson [18] in 1957. He defined a growth factor α which essentially consists of the entropy of melting (ΔS) and a crystallographic factor ξ. The factor ξ usually varies between 0.5 and 1.0, depending on the crystallographic direction in which growth is taking place. The definition of α is:

$$\alpha = \xi \frac{\Delta S}{R}$$

where R is the universal gas constant.

α-factors <2 govern growth of rough surfaces, which grow without surface nucleation. The growth rate is often diffusion controlled. Crystals of this kind can develop a dendritic growth pattern.

With α-factors >2 the growth rate is restricted by the rate of surface nucleation. In cases where some crystallographic planes have a low α-value, a crystal may preferentially grow in these directions.

According to Hunt's and Jackson's classification the Al-Al_6Fe eutectic is of the "lamellar type". That means that both the α-aluminium and the Al_6Fe phases have low entropies of melting and grow in a non-faceted manner. (This is of course obvious for the α-phase, which easily exhibits a dendritic mode of growth.) A photomicrograph of a lamellar Al-Al_6 Fe eutectic was shown in Fig. 8. The Al-Al_3Fe eutectic grows in a "faceted-nonfaceted" way, which indicates that the Al_3Fe phase has a relatively high entropy of melting. The growth of favoured, faceted surfaces of this phase is clearly shown in Fig. 6.

Table I. *Entropies of melting and α-factors for Al, Al_3Fe, Al_6Mn and Al_6Fe*

Phase	ΔS	α/ξ
Al	2.7	1.35
Al_3Fe	4.6	2.3
Al_6Mn }	3.6	1.8
Al_6Fe }		

From the thermodynamic data collected by Hultgren *et al.* [19] the approximate values reported in Table I have been calculated. The numbers for the phase Al_6Fe have been calculated under the assumption that the heat of formation of Al_6Fe is equal to that of Al_6Mn, which is defendable as an approximation in the absence of data.

Despite all the simplifications made in developing the theory and in calculating the α-factors given in Table I, there seems to be quite a good agreement between the predictions from theory and the practical observations which have been reported above.

The iron content in solid solution

In all practical applications of aluminium and aluminium alloys the distribution of iron between matrix and intermetallic compounds plays an important role.

Most studies of the influence of iron on the properties of aluminium have naturally been made on materials of technical purity, where impurities like silicon, or alloying elements like manganese, have a pronounced influence on the phase formation and on the iron distribution in the material.

Some laboratory experiments in the pure Al-Fe system have been reported, however, and from these Altenpohl [3] concludes:

Iron additions to aluminium increase the toughness of the material.

The iron content in solid solution has a very pronounced effect on the recrystallization temperature. Blade *et al.* [20] report that 0.01 % Fe increases the recrystallization temperature $\approx 100°C$.

The iron content in solid solution influences directly, or indirectly by secondary precipitation processes, the disposition to earing properties of rolled sheet-products. It is a well known fact in the aluminium industry that the tendency for the material to develop texture in the rolling process is far more

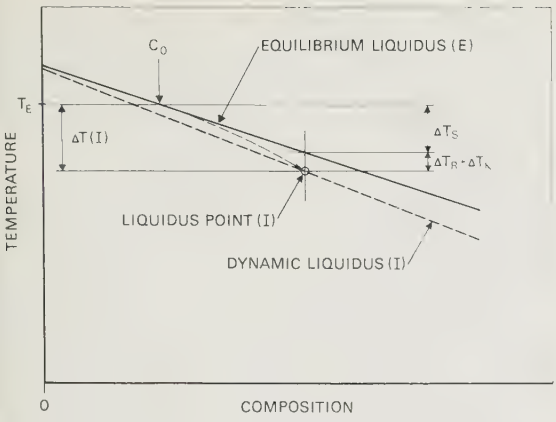

Fig. 18. The liquidus point indicates the temperature and composition of the melt in contact with the growing dendrite tip. This diagram represents a slow solidification process.

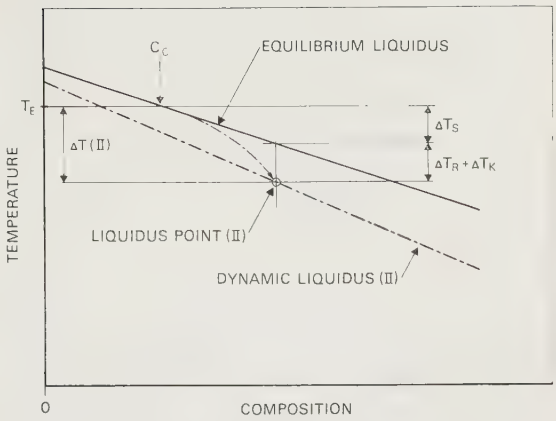

Fig. 19. The liquidus point indicates the temperature and composition of the melt in contact with the growing dendrite tip. This diagram represents a rapid solidification process.

pronounced for rapidly than for slowly solidified ingots. Trapied [21] for example, has developed a special continuous-casting technique with a slow rate of heat transfer to improve the conventional chill-casting methods.

A common opinion is that slow solidification gives low iron content in the matrix, which in turn leads to less secondary precipitation and thereby lowers the tendency for earing-sensitivity to develop.

A logical explanation of the complete mechanism of texture-development is, however, missing in the literature.

Two new views on the distribution of iron in Al-Fe alloys will be discussed in the following section.

Composition of the α-phase. It was shown earlier that the actual growth of the α-phase takes place at a certain degree of undercooling ΔT which depends on the rate of heat transfer. The ΔT is composed of three different terms ΔT_S, ΔT_R and ΔT_K. These terms cannot be separated; they are all functions of each other. It is possible, however, to estimate their relative magnitudes as the cooling rate changes.

At low rates of heat transfer the tip radius of the growing α-dendrites is large (> 10 μm). The solute build-up ahead of the tip is large and the ΔT_S component is likely to dominate over the other terms composing the total ΔT. This is schematically shown in Fig. 18.

At higher cooling rates, however, the tip radius (which is assumed to be the tip of a growing rotational paraboloid) easily decreases to the order of 1 μm. Then surface tension tends further to depress the growth temperature. At the same time the diffusion of solute in the melt around and at the growing tip can more easily take place sideways, and there is therefore rather less than more solute build-up ahead of the tip. However, as a greater ΔT is measured at higher cooling rates, the terms ΔT_R and ΔT_K will make an increasing contribution to the total undercooling. This is shown in Fig. 19.

It is not necessary that the partition ratio (k) changes with the same relative rate as the rate by which $(\Delta T_R + \Delta T_K)$ is growing. Oriani [22] has shown that the Gibbs-Thomson radius effect on composition, in cases similar to the dendritic solidification in the range of interest in this work, does not markedly change the partition ratio.

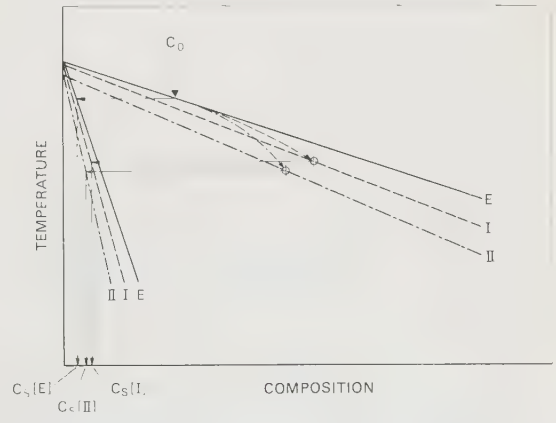

Fig. 20. Dynamic phase diagram showing the influence of cooling rate on the composition of the solid phase.

* – *Bäckerud*

Table II. *The iron content in the α-phase of samples containing 1% Fe as a function of cooling rate*

Cooling rate °C/min	% iron in the α-phase
20	0.068 ± 0.002
60	0.056 ± 0.002
150	0.050 ± 0.002

It is therefore reasonable to assume that a certain liquidus point in the phase diagram (given by the temperature and composition of the liquid in contact with the growing dendrite tips) is related to a corresponding solidus point by the partition ratio. The temperature of the solidus point is the same as the liquidus point. This is schematically demonstrated in Fig. 20, which shows the possibility for a rapidly solidified sample to grow with a lower iron content in the central parts of the α-phase, as compared to a slowly solidified sample. This hypothesis has of course to be verified by experiments.

It must first be pointed out, however, that the growth of a purer α-phase with increasing cooling rate can only be observed and thereby have practical importance in systems with a very low k value, while the diffusion of the solute atoms in the solid matrix is very slow. The Al-Fe system fulfills both of these requirements.

Samples with 1% Fe, solidified at different rates, have been analyzed by an electron microprobe. (The microstructure of such samples was shown in Figs. 5, 10 and 11).

Due to the limited geometrical resolution in the microprobe technique, very rapidly chilled samples, with a dendritic spacing $<5\mu$m, cannot be analyzed in this way. (The effective volume analyzed can be approximated with a semisphere of 4–5 μm diameter at an accelerating high tension of 20 kV and an electron beam diameter of 1 μm).

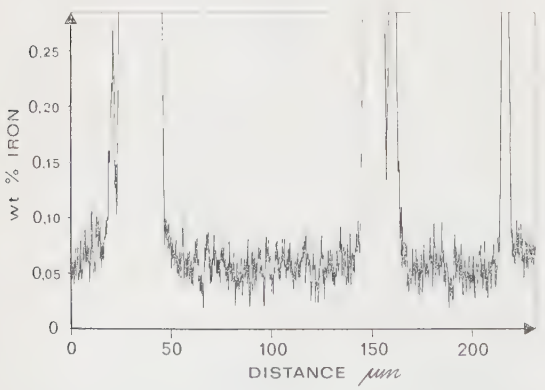

Fig. 21. Electron-microprobe line scanning across a dendrite branch showing the distribution of iron. The aluminium sample used had a nominal composition of 1% iron.

In samples solidified at three different rates, significant differences in the iron concentration in the dendrites have been measured. The results are reported in Table II.

The reported concentrations are arithmetic means of 20 measurements made in different parts of the sample. The differences obtained confirm the theory outlined above that the iron content in the aluminium matrix decreases with increasing cooling rate.

To form an idea of the iron distribution across a dendrite, the microprobe scanning shown in Fig. 21 was performed. It is seen from this figure that the iron concentration is very even across the dendrite branch.

The relative amount of α-phase. The second factor of importance in considering the iron content in solid solution is the amount of α-phase which forms at different cooling rates.

Both cooling curves and microscopic examinations indicate that the relative amount of α-phase increases with increasing rate of heat transfer during the solidification process. The relative amounts of α-phase and eutectics in the four samples shown in Figs. 5, 10, 11 and 7, which were solidified at cooling rates of 20, 60, 150 and 600 °C/min, have been determined by common metallographic technique and the results are presented in Table III. As can be seen from the reported figures, the relative amount of α-phase changes from 67 to 77% by increasing the rate of cooling within the range of common technical processes. As the properties of the α-phase are vastly different from those of the eutectics, this factor must be taken into consideration when materials produced under different casting conditions are compared.

Table III. *Relative amount of α-phase in samples with 1% Fe produced at different cooling rates*

Cooling rate °C/min	Relative amount of α-phase percent by volume
20	67
60	70
150	72
600	77

Conclusion

To conclude the observations which have been made in this study on the solidification characteristics of the Al-Fe system, the following statements can be made:

The Al-Fe system is characterized by a low partition ratio. This affects the actual temperature at which the solid phases grow. With increasing cooling rate the degree of undercooling relative to the equilibrium phase diagram is more and more pronounced.

The α-phase grows mainly in a dendritic mode.

The composition across dendritic branches is fairly constant.

The iron content of the α-phase decreases with increasing rate of cooling.

The relative amount of α-phase increases with increasing rate of heat transfer.

In samples of "dynamically" hypo-eutectic compositions two different eutectic reactions have been observed. The rate of heat transfer determines which reaction will take place.

The phase formation and growth pattern which occur in hyper-eutectic Al-Fe alloys are determined by the differences in growth kinetics between the α- and the Al_3Fe phases.

PHASE FORMATION AND GROWTH DURING THE FREEZING PROCESS OF THE BINARY SYSTEM ALUMINIUM-MANGANESE

Literature review

As seen from the general reference works by Hansen [1] and Elliott [2] aluminium-manganese alloys have been given much attention in the past. The reason for this is of course the great practical and theoretical interest these alloys have. In his review, Altenpohl [3] points out:

A manganese addition of about 1% to aluminium increases the tensile properties without changing the good corrosion resistance of the base metal.

Manganese is often added to different aluminium alloys to increase the temperature of recrystallization.

Heavy grain segregations are created during the solidification process.

There is a tendency for rolled products to obtain a very coarse-grained structure.

The principal constitution of the binary system is shown in Fig. 22. Under equilibrium conditions the eutectic reaction takes place at a temperature of 658.5°C and at a concentration of 2% manganese. The maximum solid solubility of manganese in the α-phase has been estimated to 1.4% manganese. Recent investigations, as referred to by Elliott [2], show that the solid solubility might be somewhat higher, or up to 1.8%. Due to difficulties to nucleate the second phase, however, the α-phase may easily be supersaturated. This is indicated in Fig. 22 by the dashed lines which continue the liquidus and solidus beyond the eutectic point. The second phase, which forms in the eutectic reaction, is the Al_6Mn phase, which contains around 25% manganese. The Al_6Mn phase forms directly from the melt in the concentration range between 2 and 4 % manganese. If the initial composition of the melt exceeds 4% manganese, the Al_6Mn phase if formed peritectically at 710°C by the reaction between the melt and the intermetallic compound Al_4Mn. Most alloys in practical use, however, have a manganese content of about 1%. In the present work, therefore, interest has been limited to the formation of the α- and the Al_6Mn phases. Another limitation of this work is the range of cooling rates studied. Only normal pro-

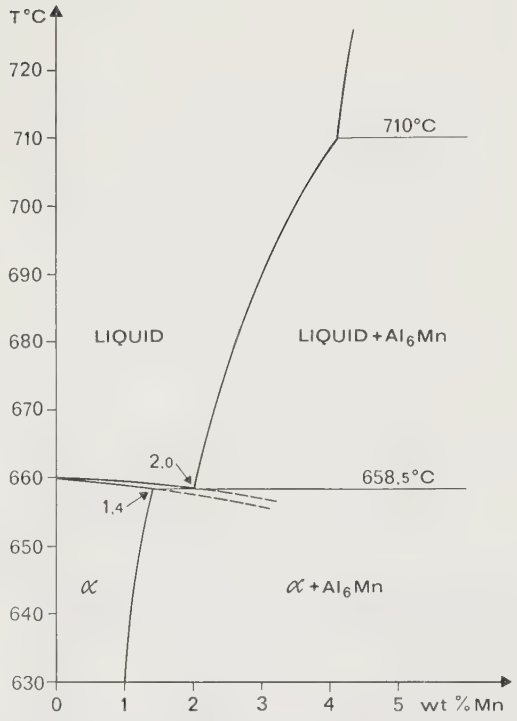

Fig. 22. Part of the aluminium-manganese equilibrium phase diagram according to Altenpohl [3].

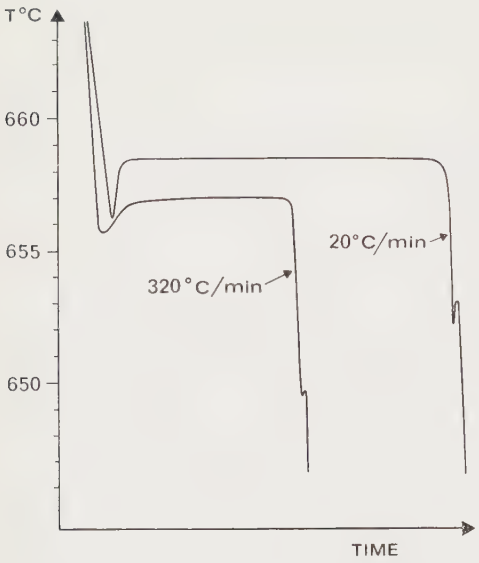

Fig 23. Cooling curves taken from aluminium samples with 1% manganese at different cooling rates. (The time scales are different in the two cases.)

duction processes have been considered, i.e. cooling rates between 1 and 1000°C per minute. In this range the α-phase always exhibits a dendritic mode of growth, which indicates that the growth process is diffusion controlled. At much higher rates of heat transfer, where diffusionless solidification takes place, it is possible to obtain very high manganese concentrations in the α-phase, as was first reported by Falkenhagen and Hofmann [23].

On the following pages some kinetic aspects of the phase formation and element distribution in the aluminium-manganese system will be treated.

Growth of the α-phase

The actual growth temperature of the α-phase as a function of rate of heat transfer in aluminium with 1% manganese, has been determined by Bäckerud [16]. The constitutional factor $(1-k)/k$ has a low value in the Al-Mn system, and technical solidification processes therefore take place not so far from the equilibrium conditions as was the case in the Al-Fe system described above. At a rate of heat transfer corresponding to 100°C/min, the actual growth temperature is depressed 1.4°C as compared to the true equilibrium diagram. The equilibrium solidification range for the Al-Mn system is, however, very narrow (1.5°C), and thus the temperature depression at actual growth rates might influence the solidification process significantly.

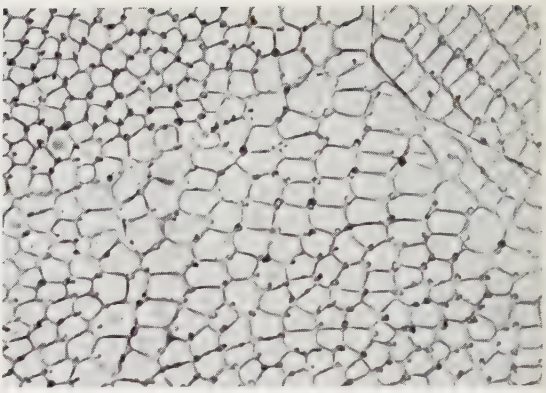

Fig. 24. The cellular dendritic structure obtained at high cooling rate (500°C/min) of an aluminium sample with 1% manganese. Etching: Keller and Dix.

The first α-phase formed grows at a constant temperature (as can be seen from the cooling curves in Fig. 23) and therefore at a fairly constant composition. The growth pattern is dendritic or cellular dendritic at all growth rates which have been investigated (see Figs. 24 and 25). The remainder of the melt which solidifies in each enclosed cell gives, due to the high k value, a small dendritic segregation. As the diffusion of manganese in the solid phase is very slow, a non-equilibrium solidification pattern (e.g. as described by Brody and Flemings [24]) will in a reasonable way represent the elemental distribution within a cell. The amount of solid formed as a function of temperature is shown in Fig. 26. The curve in this figure is based on a simplified equilibrium diagram with straight phase boundaries and is calculated from the formula:

Fig. 25. Microstructure of slowly cooled (2°C/min) aluminium sample with 1% manganese. Etching: Keller and Dix.

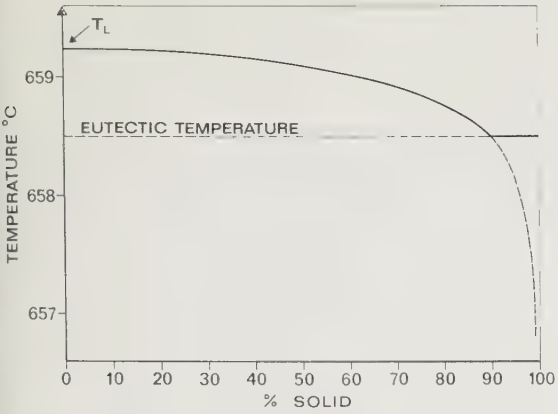

Fig. 26. The amount of solid formed as a function of temperature according to eq. (3).

$$f_S = 1 - \left(\frac{T_M - T_L}{T_M - T}\right)^{1/(1-k)} \qquad (3)$$

where f_S is fraction solid, T_M is the melting point of pure aluminium = 660.00°C, T_L is the liquidus temperature (for 1% Mn) = 659.25°C, T is the actual temperature, and k is the partition ratio = 0.7

According to eq. (3) and the constants given above the amount of melt available for formation of the eutectic is 10% of the initial volume. This means that the concentration of manganese in the 90% solid formed at this moment, according to the equilibrium diagram, may vary from 0.7 to 1.4%.

Microprobe line scannings over the dendritic structure show less segregation than expected from these calculations. This is demonstrated in Figs. 27 and 28, which show the microdistribution of manganese in two samples solidified at very different cooling rates (500°C/min and 2°C/min). From the curves it is therefore reasonable to assume that the effective k value is higher than earlier proposed, say around 0.8. There is obviously no significant difference in the segregation ratios between the rapid and the slow solidification cases.

This assumption is supported by recent measurements of solid solubility of manganese in aluminium as referred to by Elliott [2]. The possibility of a higher k value, together with the observation that the amount of α-phase increases with increasing rate of heat transfer (see page 118), and further considering the fact that limited diffusion of Mn in the solid α-phase during the solidification process may occur to some extent, will make it clear that the amount of melt at eutectic composition can become far less than the 10% calculated from eq. (3).

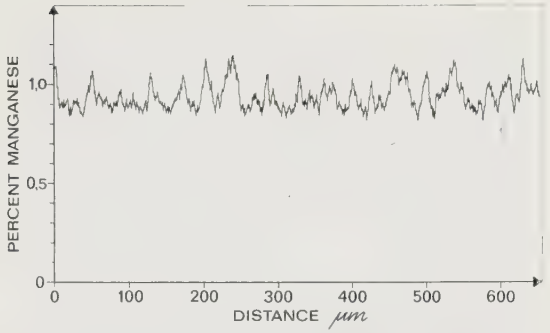

Fig. 27. Electron-microprobe line scanning showing the distribution of manganese in the sample shown in Fig. 24.

Due to microsegregations there will be in each cell a region with a high manganese content, where the second phase in the eutectic will or will not precipitate depending on the nucleation probability. Anyhow this region will be very small, as the eutectics which can be observed metallographically are extremely narrow and no indication of a very high Mn-concentration in these regions can be detected by the microprobe. (If the eutectic region should occupy 10% of the volume, the geometrical resolution of the microprobe is good enough to give intensities far above the curves shown in Figs. 27 and 28.)

The cooling curves in Fig. 23 also indicate that the formation of the eutectic takes place during a very short period of time, as compared to the total solidification time. At the temperatures of formation of the second phase found from the curves in Fig. 23 there must also be very small amounts of melt remaining in the structure, as can be calculated by eq. (3) or extrapolated from the curve in Fig. 26.

Formation and growth of the intermetallic phase Al_6Mn

The intermetallic phase Al_6Mn is most likely to occur in commercial aluminium-manganese alloys.

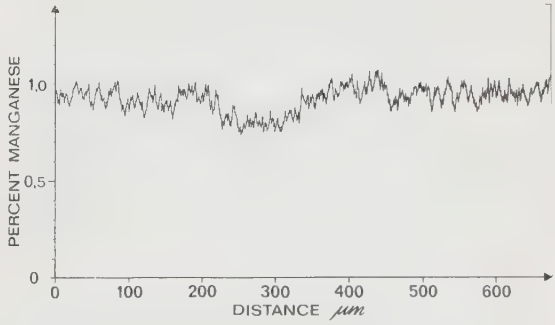

Fig. 28. Electron-microprobe line scanning showing the distribution of manganese in the sample shown in Fig. 25.

×150

Fig. 29. 12°C/min.

Hanemann and Schrader [25] report on the formation of the phase Al_4Mn in samples solidified very rapidly. Within the range of composition and solidification rates studied in this work, however, the only intermetallic phase which has been identified is Al_6Mn. As pointed out in the previous section this phase forms only with difficulty from melts with a composition below the eutectic.

The phase formation and elemental distribution in samples solidified at different rates from hypereutectic composition, have been investigated in a series of samples, all with a manganese content of 3.05%.

The first sample was allowed to solidify slowly with a cooling rate of 12°C/min. The structure obtained in this sample is shown in Fig. 29. During the slow solidification process a limited number of Al_6Mn particles have been nucleated. These particles have grown into their characteristic faceted form. During the first part of this very slow solidification process, neither the diffusion of manganese in the liquid phase nor the rate of the crystal surface reaction, have limited the growth of the Al_6Mn particles. So when the "dynamic" eutectic temperature is reached, the melt has the proper eutectic composition. From this melt the α-phase nucleates and starts to grow with a manganese concentration which has been determined by microprobe analysis to 1.6% Mn. This is in agreement with the expected composition according to the arguments given in the preceding section about the maximum solid solubility of manganese in aluminium. The α-phase exhibits as usual a dendritic, diffusion-controlled growth pattern, and manganese will concentrate in the interdendritic areas. The growth mechanism here is the same as in the solidification of a melt with hypoeutectic composition. The same difficulty to nucleate the second phase in the eutectic leads to a segregation of manganese to the last parts of the solid to be formed. However, eutectic regions can hardly be observed in Fig. 29, and the cooling curve shows no arrest point corresponding to the formation of a eutectic. Neither do the microprobe scannings give any evidence of the existence of a secondary precipitate.

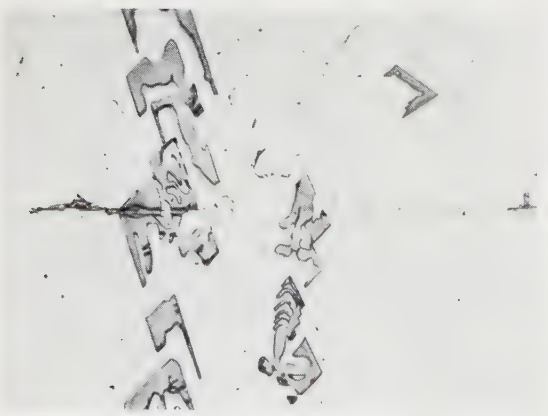

×150

Fig. 30. 110°C/min.

Fig. 29–30. Microstructure of aluminium samples with 3% manganese solidified at different cooling rates. Etching: 0.5% HF.

The microstructure of another sample which was produced at a cooling rate of 110°C/min is shown in Fig. 30. Also this sample shows primary nucleation and growth of Al_6Mn particles. Due to the high rate of heat extraction, however, the particles have been restricted in their growth, so that the "dynamic" eutectic temperature was reached and the α-phase started to grow, before the excess manganese content of the original melt had time to diffuse to the growing Al_6Mn particles and time had been allowed for the surface reaction to take place. The manganese content of the α-phase which started growing was 1.85%. By using the partition ratio of 0.8, as earlier proposed, this manganese concentration in the solid phase corresponds to a "dynamic" eutectic composition of 2.3% manganese. By starting the growth of the α-phase from the melt of this composition, the manganese content of the enriched regions in the interdendritic spacings will soon be high enough for the eutectic reaction (i.e. nucleation and growth of secondary Al_6Mn particles) to take place. This can be observed in Fig. 30 and also seen from the microprobe scanning over the same sample in Fig. 31. The cooling curve obtained from this sample is

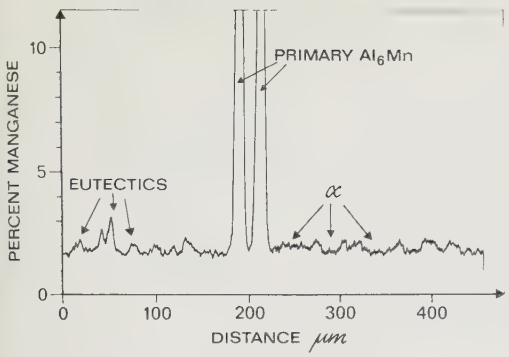

Fig. 31. Electron-microprobe scanning over the sample shown in Fig. 30, showing the distribution of manganese.

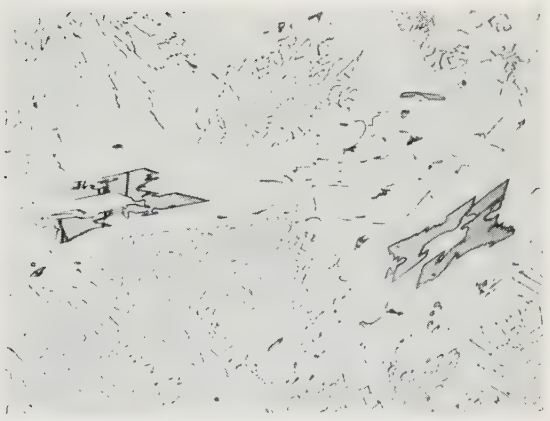

Fig. 33. Microstructure of aluminium sample with 3% manganese solidified at a cooling rate of 500°C/min. Etching: 0.5% HF.

shown as the upper curve in Fig. 32. This curve shows the initial undercooling before the nucleation of the primary Al_6Mn phase and the growth of the primary particles, which continues for nearly half of the total solidification time. Then follows a more horizontal portion of the cooling curve which indicates growth of the α-phase and finally a smooth bending downwards of the cooling curve, indicating that freezing of a heavily enriched liquid is taking place, eventually accompanied by some formation of eutectic.

The middle curve in Fig. 32 has been measured on a sample with a cooling rate of 500°C/min. Also on this curve the intial supercooling before the nucleation and growth of the primary Al_6Mn particles can be observed. The time of growth for these primary particles is, however, much less than in the foregoing example, or about 1/4 of the total solidification time. After this period of time the α-phase starts to grow, and finally a very clear arrest in the cooling curve indicates the formation of eutectics. These different stages of the solidification process are very clearly demonstrated in Fig. 33. The manganese concentration in the original α-phase regions, which developed around the primary Al_6Mn-particles, was, according to microprobe analysis, 2.35% Mn. This means that the liquid composition at the moment when the α-phase started to grow must have had an average manganese content of 2.95%. As the original composition of all the samples described in this section was 3.05% Mn, in this case only 0.1 wt% manganese is tied to the primary particles. Due to the very high supersaturation of the melt after some α-phase has been formed, favourable conditions for the formation of a true eutectic have been created. In the microprobe line scanning diagram in

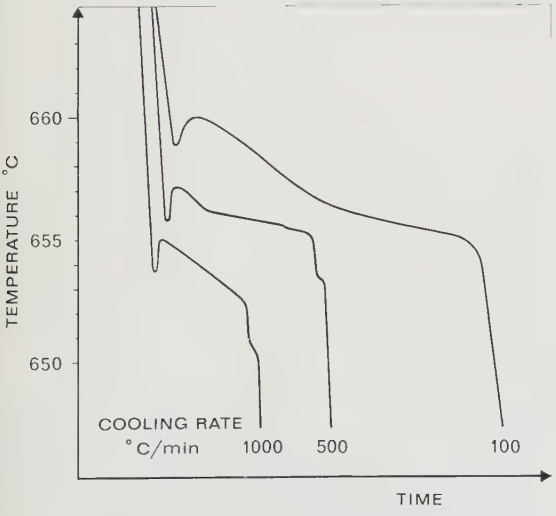

Fig. 32. Cooling curves from aluminium samples with 3% manganese measured at different rates of heat transfer.

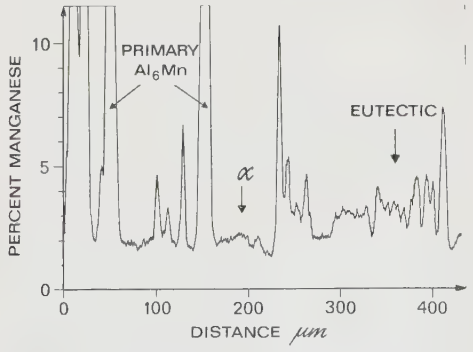

Fig. 34. Electron-microprobe scanning over the sample shown in Fig. 33, showing the distribution of manganese.

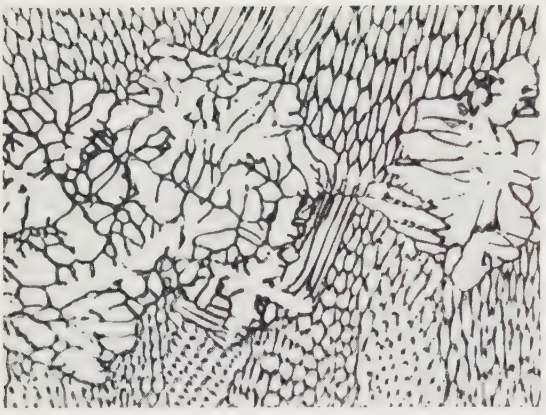

· 150

Fig. 35. Microstructure of aluminium sample with 3 % manganese solidified at a cooling rate of abt. 1000°C/min. Etching: 0.5 % HF.

Fig. 34, the different regions in Fig. 33 can be recognized: Primary Al_6Mn particles, original α-phase and the eutectic areas.

Finally a sample with a cooling rate of about 1000°C per minute was examined. The cooling curve obtained from the sample is shown as the lower curve in Fig. 32. Obviously there was not time enough for primary nucleation and growth of the Al_6Mn phase. The supercooling was high enough to reach a "dynamic" eutectic temperature, where the α-phase nucleates directly and starts to grow. The microprobe analysis of this first α-phase to form shows that its composition is around 2.9 % Mn. In the interdendritic areas the manganese concentration will fairly soon reach high values due to the segregation, and secondary Al_6Mn particles will form. This is indicated in the cooling curve by a very pronounced temperature arrest. The microstructure of this sample is shown in Fig. 35.

Discussion of phase formation and growth mechanisms in the aluminium-manganese system

As has been repeatedly pointed out in this chapter the Al_6Mn phase nucleates with great difficulty. On the other hand, when the Al_6Fe phase was discussed, it was proposed that the α-phase acted as a potential nucleant.

The apparent difference between the two systems depends on the difference in the partition ratios and consequently on the constitutional undercooling factor $(1-k)/k$. Consider two samples with 1 % of iron and of manganese, respectively. As can be found by extrapolation of the curve in Fig. 4 (or calculated from eq. (1)), the undercooling at which the α-phase in the iron-containing sample grows, at a cooling rate of 300°C/min, amounts to $\Delta T_{Fe} = 10$°C. The temperature of growth can be estimated to 659 – 10 = 649°C. In the manganese-containing sample the corresponding growth temperature, according to the lower curve in Fig. 23, is 657°C.

If the strain-energy term is neglected, Turnbull's and Vonnegut's [26] derivation of the critical Gibbs free energy of heterogeneous nucleation (ΔG^*) can be simplified to:

$$\Delta G^* = \frac{A \cdot \sigma^3}{(\Delta S \cdot \Delta T)^2}[f_1(\sigma) + f_2(\delta)]^2 \qquad (4)$$

where A is a geometrical shape constant, σ is the surface energy between nucleus and melt, ΔS is the entropy of melting, $f_1(\sigma)$ is a function of all surface energies in the system, and $f_2(\delta)$ is a function of the disregistry (misfit between nucleus and nucleant).

It is reasonable to assume that all the factors defined above are very similar in the nucleation processes of Al_6Mn and Al_6Fe. We can therefore state that

$$\Delta G^* \sim \frac{1}{(\Delta T)^2} \qquad (5)$$

The lower cooling curve in Fig. 23 shows that the Al_6Mn phase is nucleated at a temperature just below 650°C, which is the same temperature as earlier reported for the nucleation of the Al_6Fe phase.

The growth of Al_6Mn particles from hyper-eutectic melts can be restricted by two different mechanisms.

As seen from the experiments performed in the previous section, a limited number of Al_6Mn particles seem to nucleate and grow. As the temperature rises rapidly after the initial undercooling of the melt, further nucleation is unlikely to occur. The growth of the Al_6Mn particles may be restricted by the very low diffusion rate of manganese atoms in the melt. Another possibility is that the growth rate is limited by a slow surface reaction. Jackson's α-factor for Al_6Mn was estimated to $\alpha_{Al_6Mn} = \xi$ 1.8, as reported in Table I, and this indicates that the crystal surfaces should grow without a nucleation energy barrier to be overcome. On the other hand, the Al_6Mn crystals grow in a typical faceted manner, which often means that the growth is taking place stepwise.

From microprobe line scannings, like that in Fig.

34 a small concentration dip is often found in the immediate vicinity of the primary Al_6Mn particles. At larger distances from the particles the average manganese concentration is found to be very high. These observations show that the growth of the primary Al_6Mn particles is controlled mainly by the slow diffusion rate of manganese in the melt.

Under most technical casting conditions, the rate of heat transfer is higher than the diffusion rate of manganese. The heat transfer will therefore control the development of the structure, as was experimentally demonstrated in the previous section.

Conclusions

The following conclusions can be drawn from the experiments reported in this chapter.

Hypo-eutectic alloys. The aluminium-manganese system has a high partition ratio, which in this work has been determined to $k = 0.8$.

The microsegregation of manganese in the major part ($> 90\%$) of the α-phase is low.

The α-phase grows at a very low degree of undercooling.

The composition of the α-phase does not change noticeably with the cooling rate.

Due to the high temperature at which the α-phase develops, the degree of undercooling necessary for nucleation of the Al_6Mn phase will not be reached until late in the solidification process. This leads to a pronounced increase of manganese in the very last portions of solid formed in the interdendritic areas.

Hyper-eutectic alloys. The low diffusion rate of manganese atoms in the melt determines the growth rate of primary Al_6Mn particles.

The rate of heat extraction controls the formation and growth habits of phases.

A true eutectic reaction in the aluminium-manganese system has been observed only when melts of hyper-eutectic composition solidify within a limited range of cooling rates (around 500°C/min).

THE INTERMETALLIC COMPOUND $Al_6(Mn, Fe)$

Literature review

The binary intermetallic phase in the Al-Mn system of interest in this work is the Al_6Mn phase. The principal structure and the lattice parameters of this intermetallic compound were first determined by Hofmann [27] in 1938. A detailed structure analysis was performed by Nicol [28] in 1953 and his results were verified by Taylor [29] in 1960.

Table IV. *Lattice parameters in Ångström units of the phases Al_6Mn and Al_6Fe*

Phase	*a*	*b*	*c*
Al_6Mn	6.50	7.55	8.87
Al_6Fe	6.49	7.44	8.79

It was early observed that the manganese in the Al_6Mn compound could be replaced atom for atom by iron up to about 50% substitution. Degischer [30] found the composition of the iron-saturated phase to be 14% Mn and 13% Fe, that means a substitution of 48%. (Assuming that the analytical errors in the chemical determination of both components are equal.)

Phragmén [31] produced $Al_6(Mn,Fe)$ crystals which were in equilibrium with Al_3Fe, and which contained 12% Mn and 14.6% Fe, that means with a substitution of 55%. He concluded that the maximum degree of substitution is near 50%. The same conclusion has been made by Phillips [32] and Raynor [33].

In 1962 Hollingsworth *et al.* [10] reported the discovery of a new phase, Al_6Fe, formed in rapidly chilled ingots containing 2% iron in aluminium of high purity. The structure of this phase was investigated by Walford [11], who found it to be isostructural with the Al_6Mn phase.

The lattice parameters of the two binary phases, according to Nicol and to Hollingsworth *et al.*, are given in Table IV.

Experiments

Small ingots with 3–4% Mn and varying Fe content were slowly pulled through a vertical furnace in a graphite crucible, using a technique similar to that used in the growing of single crystals by Bridgman. Needle-shaped crystals of the $Al_6(Mn,Fe)$ type with different Mn/Fe ratios could be separated from the matrix by a conventional anodic dissolution technique in a dilute mixture of hydrochloric and nitric acids (2:1).

Chemical analyses of the separated particles showed that the degree of Fe substitution in the crystals varied from 0 to 64%. The highest degree of substitution was obtained in a sample from a melt with the composition 1% Mn and 3% Fe.

Electron microprobe analysis of the particles in

Table V. *Composition of $Al_6(Mn,Fe)$ particles*

Sample No.	Isolated particles			Particles in situ % substitution
	At % Mn	At % Fe	% subst.	
1	14.3	0	0	0
2	13.1	1.2	8	10
3	12.1	2.2	15	—
4	11.2	3.1	22	24
5	8.4	6.0	42	41
6	7.1	7.2	50	—
7	5.2	9.2	64	63

situ showed very good agreement with the chemical analyses of the separated particles, as shown in Table V.

The microprobe analyses of the particles in situ showed that they are homogeneous in composition within the analytical error of ±2% relative. The analyses of different particles in the same sample gave a somewhat broader distribution, but well within ±5% relative.

The compositions reported in Table V have been plotted in a ternary phase diagram in Fig. 36. It is obvious from this figure that there can be a continuous substitution ranging from the Al_6Mn towards the Al_6Fe composition. A higher degree of substitution than the 64% as obtained in this series of experiment has not previously been reported in the literature.

Diffractograms were taken from all the samples in Table V by means of a Philips diffractometer PW

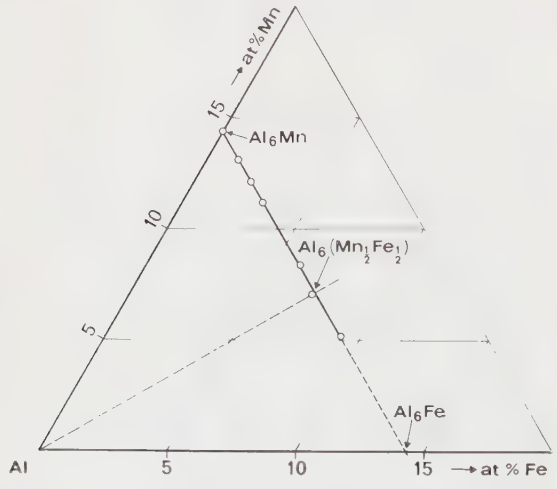

Fig. 36. The aluminium-rich corner of the aluminium-manganese-iron phase diagram. The compositions of isolated crystals of the $Al_6(Mn, Fe)$ type are indicated.

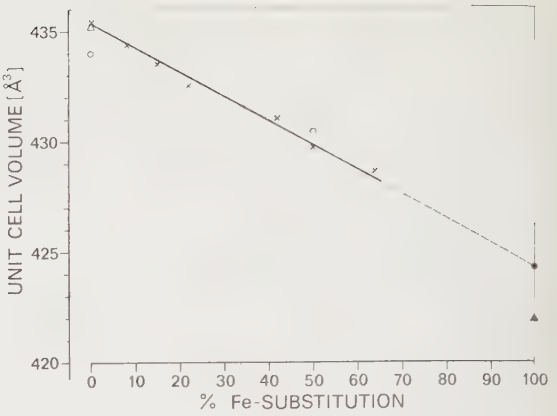

Fig. 37. Unit cell volumes of crystals of the $Al_6(Mn, Fe)$ type.
△ according to measurements by Nicol [28].
○ according to measurements by Phragmén [31].
● according to measurements by Hollingsworth *et al.* [10].
▲ according to measurements by Walford [11].
× measured in this work.

1050. Clean diffractograms were obtained, where all peaks could be identified according to the ASTM-index card.

No significant intensity changes between the diffraction peaks could be observed with the change in Mn/Fe ratio. This ratio, however, had a clear influence on the lattice parameters. The diffraction technique used is not suitable for high precision measurements of lattice parameters, but the values obtained indicate that there is a continuous and linear decrease in the parameters with increasing Fe content in the phase. This is demonstrated in Fig. 37. The values given by Nicol, Phragmén, Walford and Hollingsworth *et al.* are also indicated in the diagram. The values obtained in this work are in good agreement with those given by Nicol and Hollingsworth *et al.* Phragmén's values fit reasonably well to the curve in Fig. 37, but the cell volume calculated from the parameters given by Walford falls far below the curve.

From the literature and from the observations made above, it is obvious that the Al_6Mn phase readily takes up iron in substitutional solution, and that a degree of substitution around 50% seems to have a maximum stability.

The reason for this maximum stability of the phase with 50% iron substitution could possibly be an ordering effect between iron and manganese atoms in the crystal structure. An ordering effect cannot be detected by x-ray diffraction technique due to the very small difference in x-ray scattering power of

the manganese and iron atoms. The neutron scattering power of the two atoms, however, is very different, and neutron diffraction seemed to be a useful tool to investigate the possible existence of an ordering effect.

Neutron diffractograms were taken from samples of the $Al_6(Mn,Fe)$ type with 0, 25 and 50% iron in substitution, using thermal neutrons monochromatized to $\lambda = 1.07$ Å. Parts of the diffractograms are shown in Fig. 38. All diffraction lines have been identified and indexed and are shown to belong to the Al_6Mn type of crystal. As no other low angle lines appear with increasing iron substitution, no ordered structure having a larger unit cell than the Al_6Mn cell seems to be formed.

It is obvious from the diffractogram that the relative intensities of the diffraction lines change with increasing iron substitution. A complete structural analysis, considering all possible sites for the iron atoms in the crystal, is a complicated matter. No efforts have been made to treat this problem. In an indirect way, however, the question whether some kind of ordering exists or not in the substituted structure has been treated.

The structure factors (F_c) were calculated under the assumption that the iron atoms are completely randomly distributed among the initial manganese sites in the structure. The space group was considered to be Cmcm, the atomic parameters determined by Nicol [28] were used, and the neutron scattering amplitudes were obtained from the International tables of x-ray crystallography.

The calculated variation in the values of the $(F_c)^2$, with increasing iron substitution is found to be in agreement with the observed intensity variations in the neutron diffractograms.

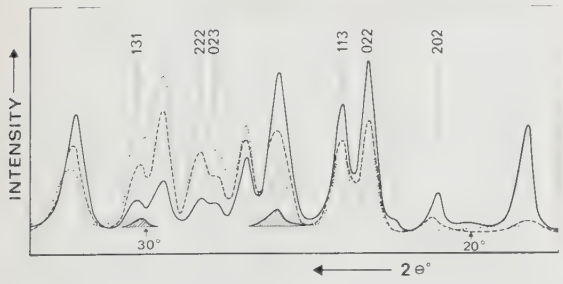

Fig. 38. Part of neutron diffractogram obtained from samples of $Al_6(Mn,Fe)$ type. $\lambda = 1.07$ Å.
——— Al_6Mn
– – – – $Al_6(Mn_{0.75}Fe_{0.25})$
. . . . . $Al_6(Mn_{0.5}Fe_{0.5})$

The neutron diffraction analysis therefore gives no indication towards the existence of an ordering effect with increasing iron content in the phase $Al_6(Mn,Fe)$.

SOME KINETIC ASPECTS OF PHASE FORMATION AND GROWTH PROCESSES DURING THE SOLIDIFICATION OF ALUMINIUM-MANGANESE-IRON ALLOYS

Introduction

Aluminium-manganese alloys are widely used especially in sheet products. The strength of the material is about 20% higher than for commercially pure aluminium, and the alloy type has a good corrosion resistance.

The most common alloy contains 1–1.2% manganese, around 0.5% iron and some silicon.

Altenpohl [3] concludes in his review:

The composition of the alloy has to be controlled within narrow limits if optimum properties of the alloy are to be developed.

Direct-chill cast ingots contain manganese in highly supersaturated condition. The segregations of manganese in the structure are very pronounced. Only by an effective heat treatment (homogenization) for a long period of time at temperatures above 600°C can these segregations be evened out.

The presence of iron is said to decrease the solid solubility of manganese in the matrix.

A considerable amount of manganese is tied to intermetallic compounds with silicon and iron.

The particles containing manganese and iron, which are formed during the freezing process, are very stable and often impossible to dissolve in the structure, even at very long heat treatments at elevated temperatures.

Increasing the iron content in alloys with 1.2% manganese governs the development of better tensile properties.

If the iron content exceeds 0.6–0.7% however, hard crusts will appear in the material.

The iron content of the alloys should, however, be kept just above 0.5% to facilitate the development of a fine-grained recrystallized structure by the heat treatment of cold rolled sheet.

In the following part of this work, phase formation and growth mechanisms will be investigated in the ternary system aluminium-manganese-iron and the distribution of elements between different

×100

Fig. 39. No iron.

×100

Fig. 41. 0.65% iron.

phases as a function of solidification characteristics will be discussed.

Experimental study of phase formation and growth

Hypo-eutectic alloys. A series of experiments was performed to investigate the element and phase distribution existing in samples of hypo-eutectic alloys (according to the binary aluminium-manganese system), which were solidified extremely slowly and were kept at elevated temperatures for a long time. Such samples, which can be assumed to have reached a "technical equilibrium" state, were produced in the same Bridgman type of furnace as was used for growing $Al_6(Mn,Fe)$ crystals.

The cooling rate was around 2°C/h in the temperature region 700–600°C. After having reached the latter temparature, the samples were quenched in water.

All samples contained 1.15% manganese, and the iron content varied from 0 to 1.15%. The microstructures of four representative samples are shown in Figs. 39–42, and the analytical results from chemical determinations and microprobe measurements are reported in Table VI.

It is obvious from the analytical results and from the micrographs that the iron content of the alloy controls the formation of intermetallic phases and thereby influences the composition of the matrix. At all compositions studied, the $Al_6(Mn,Fe)$ phase forms with a degree of iron substitution equal to 50%, which clearly indicates that the phase has its lowest free energy and therefore its highest stability at this degree of substitution.

The results from these experiments with very low cooling rate can be summarized in the following way.

Iron additions to an aluminium-manganese alloy causes the formation of the intermetallic compound

Fig. 39–42. Very slowly solidified aluminium samples with 1.15% manganese and different iron contents. Unetched.

×100

Fig. 40. 0.3% iron.

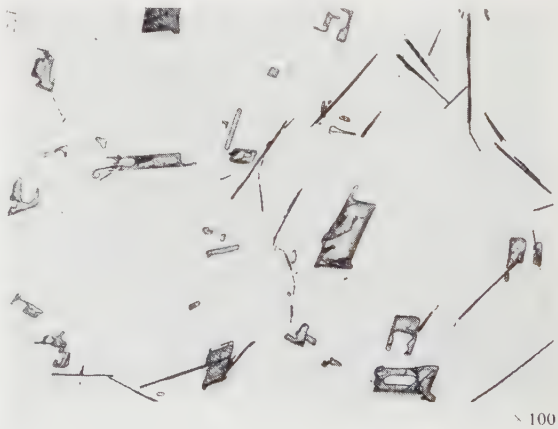

×100

Fig. 42. 1.15% iron.

Table VI. *Composition of matrix and intermetallic compounds in slowly solidified samples with 1.15% manganese and varying iron content*

Composition of the melt		Composition of the matrix		Composition of intermetallics[1]	
% Mn	% Fe	% Mn	% Fe	% Mn	% Fe
1.15	0.0	1.15	0.0	12.6	12.6
1.15	0.30	0.9	0.0	12.6	12.6
1.15	0.65	0.5	0.0	12.6	12.6
1.15	1.15	0.5	0.0	12.6 3	12.6 38[2]

[1] There is naturally a statistical variation in the analytical results obtained from individual particles in one and the same sample, but the 50% substitution of manganese by iron in the $Al_6(Mn, Fe)$ phase has been clearly verified in each case.
[2] This is the Al_3Fe phase.

$Al_6(Mn,Fe)$, which always develops in its iron-saturated form with 50% of the manganese atoms substituted by iron atoms.

By forming this $Al_6(Mn_{\frac{1}{2}}Fe_{\frac{1}{2}})$ intermetallic compound, the manganese content of the matrix is decreased by an amount corresponding to the amount of iron added.

This process goes on until that concentration of manganese in the matrix is reached where the chemical potential of manganese in the α-phase equals that in the intermetallic compound, and the reaction therefore ceases. This manganese concentration is found to be $\approx 0.5\%$.

Excess iron added to the samples precipitates in the form of Al_3Fe crystals. Microprobe analysis shows that $\approx 7\%$ of the iron atoms in the Al_3Fe phase can be substituted by manganese atoms.

Part of a microprobe line scanning over the matrix and some intermetallic particles in the sample shown in Fig. 41, are reproduced in Fig. 43.

Another series of experiments has been performed to study the influence of cooling rate (within the range of technical interest) on the phase formation and growth processes in the aluminium-manganese-iron system.

All samples in these experiments had a composition of 1.1% manganese and 0.5% iron.

Samples of 75 g weight were melted in graphite moulds in the same way as described earlier. Typical cooling curves are presented in Fig. 44, and the microstructures of four samples, solidified with cooling rates of 500, 100, 20 and 2°C/min, are shown in Figs. 45–48. As can be seen from the micrographs

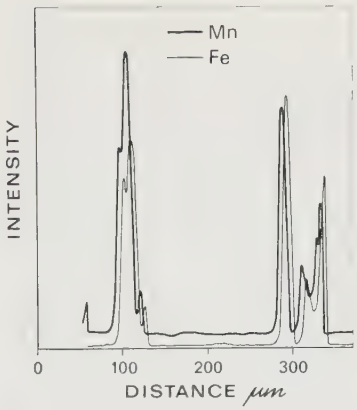

Fig. 43. Electron-microprobe scanning over the sample in Fig. 41, showing the manganese and iron distribution.

there is a remarkable change in the microstructure with the change in cooling rate.

The finely dispersed eutectic shown in Fig. 45 is very similar to the Al_6Fe eutectic developed at high cooling rates in the binary aluminium-iron system shown in Figs. 7 and 8.

With decreasing cooling rate the eutectic grows coarser (Fig. 46), it changes its morphology (Fig. 47), and finally, at a low cooling rate, $Al_6(Mn, Fe)$ particles develop their characteristic growth habit, (Fig. 48).

From the two cooling curves in Fig. 44 it is obvious that the α-phase grows with an undercooling (ΔT) which is somewhere between the values which were obtained from the two binary systems earlier investigated. At the cooling rate of 20°C/min the α-

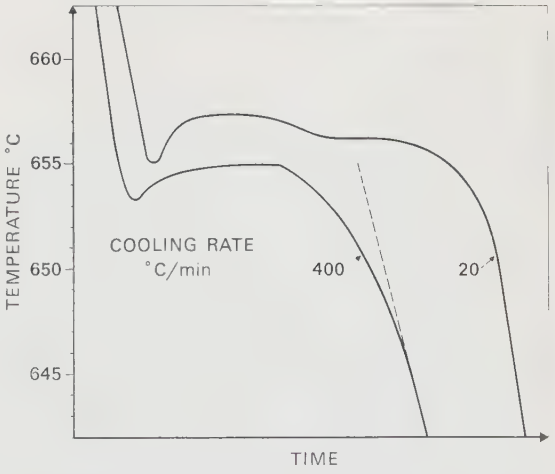

Fig. 44. Cooling curves from aluminium samples containing 1.1% manganese and 0.5% iron, solidified at different rates. (The time scales are different.)

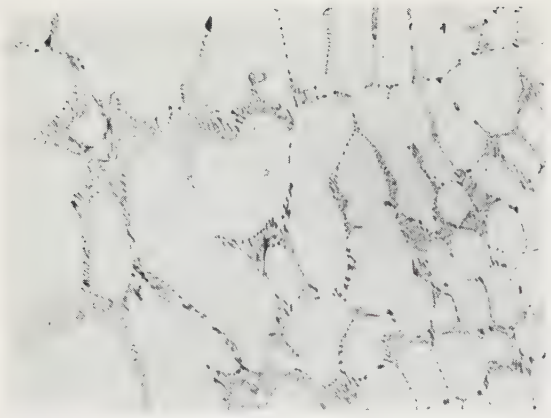

× 400

Fig. 45. 500°C/min.

× 400

Fig. 47. 20°C/min.

phase grows at a temperature of 657°C, and a ternary eutectic reaction seems to take place at a temperature of 656°C. The smooth bending downwards of the cooling curve after the arrest plateau shows that the solidification process continues in a melt which due to segregation is enriched in alloying elements. It is possible that the growth rate of the intermetallic compound in the eutectic is limited by the slow diffusion rate of manganese atoms in the melt.

The lower cooling curve in Fig. 44 indicates a similar growth pattern. The α-phase at this high rate of 400°C/min develops at a temperature of 655°C. This temperature is well below the eutectic plateau measured in the slower cooling case. As no temperature arrest can be detected in this case, the eutectic may already have nucleated and started the growth process before the end of the α-phase plateau. The remaining part of the melt solidifies apparently in a continuous growth process at falling temperatures between 655 and 645°C.

The intermetallic phases formed in all samples in this series of experiment have been identified by x-ray diffraction technique and shown to belong to the $Al_6(Mn,Fe)$ type. No other intermetallic compound has been found.

It is of course of great interest to see if the composition of the $Al_6(Mn,Fe)$ phase depends on the cooling rate.

Microprobe line scannings have been made over the structures shown in Figs. 45–48. The results of these measurements are shown in Fig. 49.

As the intermetallic particles are very small in the rapidly solidified samples, they occupy only a minor part of the effective x-ray emitting volume recorded in the microprobe. The two recording channels of the instrument were, however, calibrated to give equal intensities for equal concentrations of man-

Fig. 45–48. Microstructure of aluminium samples with 1.1 % manganese and 0.5 % iron, cooled at different rates. Etching: 0.5 % HF.

× 400

Fig. 46. 100°C/min.

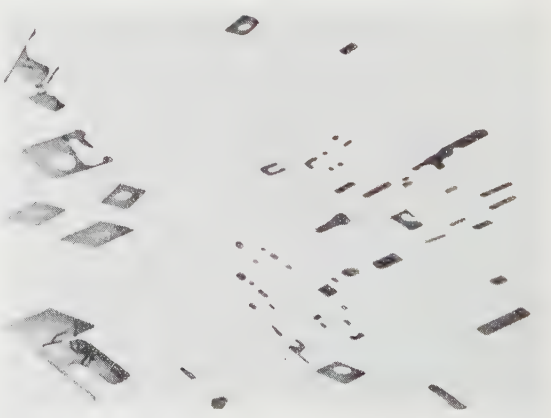

× 400

Fig. 48. 2°C/min.

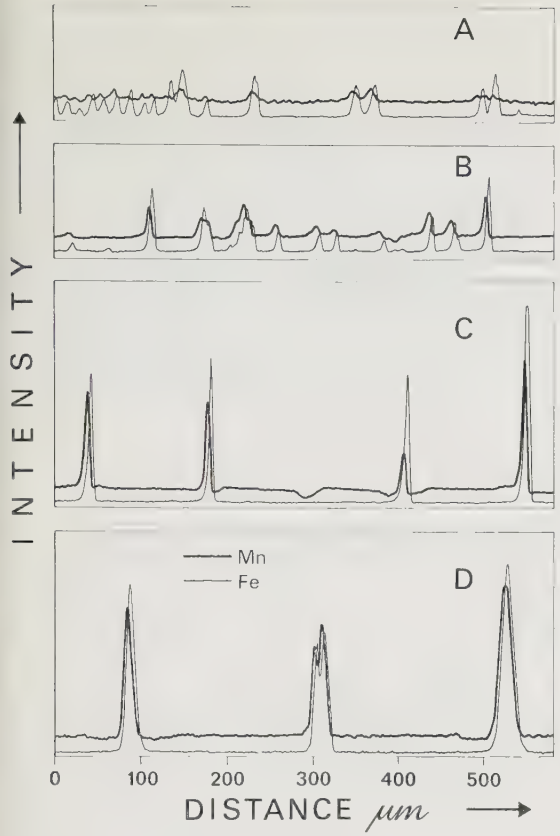

Fig. 49. Microprobe scannings showing the manganese and iron distribution in the samples shown in Figs. 45–48. The cooling rates are: A) 500°C/min; B) 100°C/min; C) 20°C/min; D) 2°C/min.

ganese and iron. This is possible for these two elements which have very similar excitation and absorption characteristics.

The two curves in each diagram therefore give the true relation between the manganese and iron concentration in the particles. (There is a small horizon-

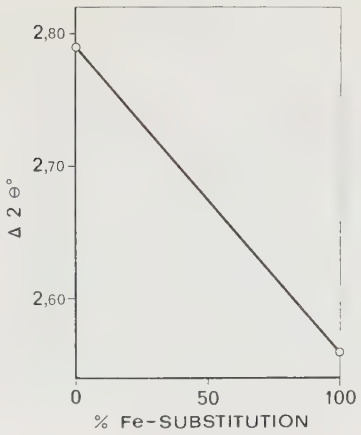

Fig. 50. The change in position between the $Al_6(Mn,Fe)$ (222) and the Al(200) reflexions as a function of percent iron substitution in the $Al_6(Mn,Fe)$ phase.

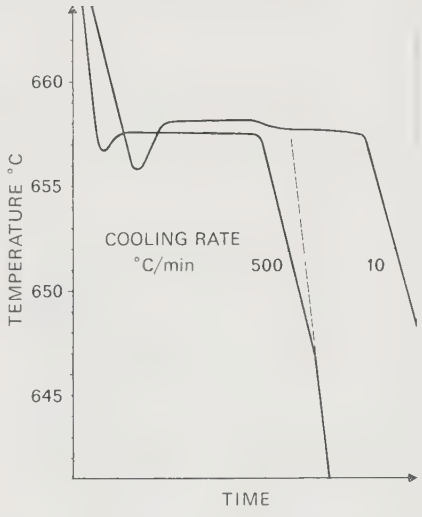

Fig. 51. Cooling curves from aluminium samples with 3 % manganese and 0.15 % iron, at two different cooling rates. (The time scales are different.)

Table VII. *Results of x-ray diffraction measurements to determine the iron content in the intermetallic compound $Al_6(Mn, Fe)$*

Sample composition		Cooling rate	Mn in matrix	Measured 2θ value for Al(200)	Correction in 2θ value for Al(200)	Corrected 2θ value for Al(200)	Measured 2θ value for Al_6Mn(222)	Δ2θ	Fe in substitution
%Mn	%Fe	°C/min	%	degrees	degrees	degrees	degrees	degrees	%
1.1	0.5	500	1.0	44.73	−0.04	44.69	42.09	2.60	83
1.1	0.5	100	0.9	44.81	−0.03	44.78	42.16	2.62	74
1.1	0.5	20	0.8	44.81	−0.03	44.78	42.14	2.64	65
1.1	0.5	2	0.7	44.80	−0.03	44.77	42.09	2.68	48
3.05	0	12	1.6	44.78	−0.06	44.72	41.93	2.79	0
0	1.0	200	0	44.70	0	44.70	42.14	2.56	100

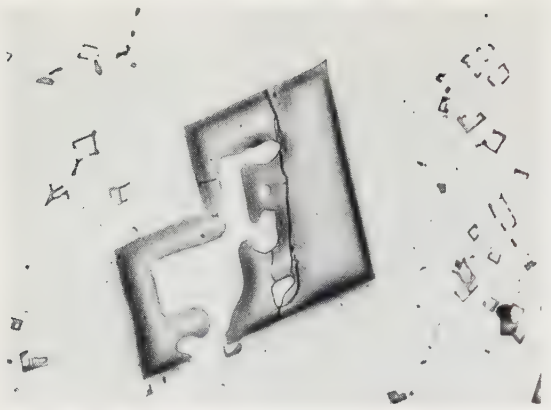

× 150

Fig. 52. 10°C/min.

× 150

Fig. 54. 500°C/min.

tal displacement between the two microprobe curves in each diagram shown in this work, due to the displacement of the two pens of the two-channel recorder used.)

It is extremely interesting to note from the curves in Fig. 49 that the iron content dominates over the manganese in the rapidly cooled samples.

Only in the slowly solidified sample represented in curve *D* of Fig. 49, the phase with 50 % iron substitution is found.

The conclusions which can be drawn from these measurements are that the $Al_6(Mn, Fe)$ phase in all technical processes has an iron content which is above 50 % substitution. (When the iron/manganese ratio > 1, the expression "iron substitution" may not be quite correct, but will be used in the remainder of this paper for the sake of simplicity.)

To support further the findings made above another set of measurements were performed. By using an x-ray diffractometer, the relative change in the lattice parameters of the $Al_6(Mn, Fe)$ phase was determined in the samples described above.

The position of the $Al_6Mn(222)$ diffraction line, which with the Cu_{K_α} radiation used was located at $2\theta \approx 42°$, was determined relative to the Al(200) line at $2\theta \approx 44.7°$.

After the reference line had been corrected for the influence of manganese in solid solution, according to the recommendations made by Pearson [34], the difference between the two lines ($\Delta 2\theta°$) was determined.

To calibrate the curve, two samples, one containing only the Al_6Mn phase and the other only the Al_6Fe phase, were measured and connected by a straight line (which is defendable according to the curve in Fig. 37).

Fig. 52–55. Microstructure of aluminium samples with 3.0 % manganese and 0.15 % iron, cooled at different rates. Etching: 0.5 % HF.

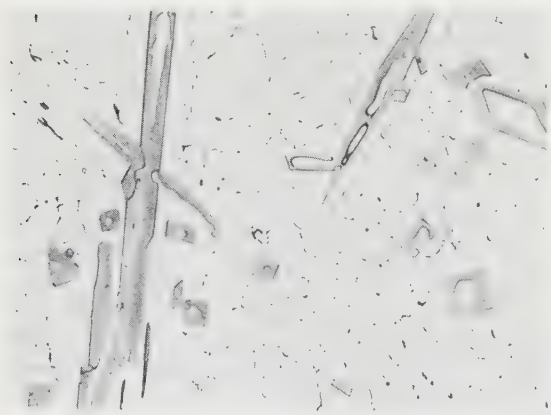

× 150

Fig. 53. 75 C min.

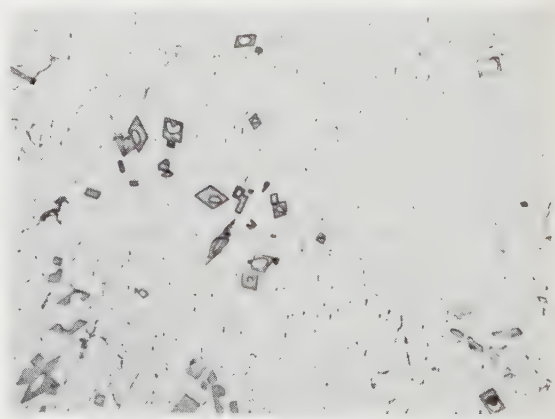

× 150

Fig. 55. 1000°C/min.

The calibration curve is shown in Fig. 50, and the measured and calculated values are reported in Table VII.

The x-ray diffraction measurements confirm the statements made above concerning the high degree of iron substitution in the rapidly chilled samples.

Hyper-eutectic alloys. The phase formation sequence and the structure development in alloys with 3.0% manganese and a small addition of iron (0.15%) have been studied. Samples were produced in the same way as described earlier. Cooling curves were recorded, the microstructures examined and the elemental distribution between the different phases determined by microprobe analysis.

The cooling curves from samples with cooling rates of 10 and 500°C/min are shown in Fig. 51. The microstructures of four representative samples, produced at cooling rates of 10, 75, 500 and 1000°C/min respectively are shown in Figs. 52–55. These micrographs should be compared to Figs. 29, 30, 33 and 35, which show the corresponding structures in the binary aluminium-manganese system.

It is obvious from the micrographs that the nucleation process both of primary and secondary precipitates is facilitated by the presence of iron.

At a cooling rate of 1000°C/min no primary Al_6Mn particles nucleated in the pure aluminium-manganese sample, but a substantial number of primary $Al_6(Mn,Fe)$ particles can be seen in Fig. 55. The manganese content of the α-phase in this sample is 1.9% compared to 2.9 in the iron-free sample.

The two samples solidified at intermediate cooling rates (from 500 and down to 75°C/min) show well developed primary and secondary precipitates of the $Al_6(Mn,Fe)$ type. The manganese concentration in the α-phase was in both these samples 1.6%.

The lower cooling curve in Fig. 51 shows the initial undercooling before nucleation and the subsequent growth of primary intermetallic crystals. When the growth of these particles has terminated, the α-phase develops and finally, in a temperature range of ≈ 10°C, the Al-$Al_6(Mn,Fe)$ eutectic forms.

At a cooling rate of 10°C/min (the upper curve in Fig. 51), the primary $Al_6(Mn,Fe)$ particles grow very large, and the secondary particles tend to become idiomorphic, as seen in Fig. 52. The manganese concentration in the α-phase region is 1.45%.

It should be mentioned that microprobe curves show that all the iron which can be detected is tied to the Al_6Mn particles. They have therefore been designated $Al_6(Mn,Fe)$ in this text, though the degree of iron substitution is less than 5%.

× 150

Fig. 56. Microstructure of an aluminium sample with 3.0% manganese and 0.5% iron, produced at a cooling rate of 1000°C/min. Etching: 0.5% HF.

To illustrate how a further addition of iron facilitates the nucleation process to a still higher extent, the microstructure of a sample with 3.0% manganese and 0.5% iron, solidified with a cooling rate of 1000°C/min is shown in Fig. 56.

Discussion of phase formation and growth in aluminium-manganese-iron alloys

The experiments performed in this work clearly show that the phase $Al_6(Mn,Fe)$ exists over the whole composition range from Al_6Mn to Al_6Fe and that it occupies its most stable condition when equal amounts of manganese and iron atoms are present, and the phase hence can be denoted $Al_6(Mn_{\frac{1}{2}}Fe_{\frac{1}{2}})$.

It is not possible to explain the stability of the $Al_6(Mn_{\frac{1}{2}}Fe_{\frac{1}{2}})$ phase by asssuming that the manganese and iron atoms occupy preferred sites in the crystal structure and thus create the highest possible degree of ordering at this intermediate composition, as no ordering of the structure could be found by the neutron diffraction measurements.

The entropy of mixing will therefore be assumed to be totally responsible for the lowering of the Gibbs free energy of the phase.

The variation of free energy (G) with composition within the $Al_6(Mn,Fe)$ phase is shown in principle in Fig. 57. The relative change in G with composition is always largest near the "pure" phases. That means, for example, that even small iron additions to the Al_6Mn phase cause a pronounced drop in the free energy of the phase, which in turn increases its sta-

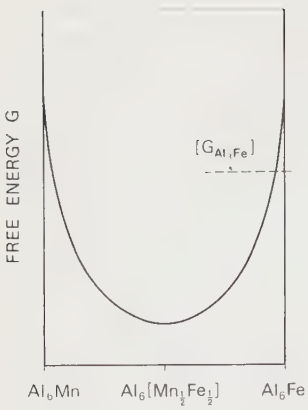

Fig. 57. Representation of the free-energy curve as a function of composition for crystals of the $Al_6(Mn,Fe)$ type.

bility, and facilitates its nucleation and growth. The difference in free energy per unit volume (ΔG_v) between the liquid and solid states will be markedly increased by the iron addition ($\Delta G_v = \Delta S_v \times \Delta T$). This will have a great influence on the critical nucleation energy ΔG^*, since, as seen from eq. (4) when writing the first factor

$$\Delta G^* = \frac{A \cdot \sigma^3}{(\Delta G_v)^2} \cdot [\quad],$$

ΔG^* is inversely proportional to the second power of ΔG_v.

This phenomenon was illustrated by comparing samples with 3% manganese and with 0.00 or 0.15% iron, where the number of nuclei drastically increased with the small iron addition. The diffusion paths in the liquid phase were considerably shortened and the growth of the intermetallic particles therefore not limited by slow mass-diffusion in the liquid phase, as was the case in the pure aluminium-manganese system.

Fig. 58. Schematic representation of solute build-up and intermetallic-phase formation ahead of growing dendrite tips.

In hyper-eutectic manganese alloys (>2% manganese) a manganese-rich $Al_6(Mn,Fe)$ phase forms primarily, and in principle all iron added to the alloy is taken up by the intermetallic compound, which can hold any composition from Al_6Mn to $Al_6(Mn_{\frac{1}{2}}Fe_{\frac{1}{2}})$. (At high supersaturation of iron the maximum degree of substitution was found to be 64%, as shown in Table V.)

In hypo-eutectic alloys (<2% manganese), the intermetallic phase which nucleates and grows is always to be found on the iron-rich side of the $Al_6(Mn,Fe)$ phase.

In aluminium-manganese-iron alloys it should be expected that the iron content, due to its high constitutional undercooling factor $(1-k)/k$, controls the degree of undercooling at which the dendritic α-phase grows. From the cooling curves, however, it is found that both the α-phase and a eutectic develop at a temperature above 655°C at intermediate cooling rates. (See for example Fig. 44.) This is close to the dynamic undercooling found for binary aluminium-manganese alloys.

A proposed growth mechanism which can account for these observations is given in the following.

Just ahead of the surfaces of the growing α-phase there will be a pronounced build-up of iron and to some extent of manganese.

The presence of manganese governs the formation of an iron-rich $Al_6(Mn,Fe)$ phase with a Gibbs free energy far below that of the pure Al_6Fe phase and below that of the Al_3Fe phase, as indicated in Fig. 57. As long as such particles grow in the enriched layer they will consume to a large extent the amount of iron rejected from the growing α-phase. This explains why the undercooling (ΔT) is much less than in the binary aluminium-iron system.

The intermetallic particles will be pushed ahead of the growing dendrites until that composition and that temperature is reached in the interdendritic areas, when a "true" eutectic reaction can take place. This mechanism is illustrated in the microstructure shown in Fig. 46, and the growth mechanism is schematically depicted in Fig. 58.

The composition of the intermetallics growing in

the enriched layer depends on the rate of heat transfer as compared to the rate of diffusion of manganese atoms in the melt (which is less than the diffusion rate of iron in liquid aluminium by at least a factor of 5). The rate of growth of the particles is mainly controlled by the rate of diffusion of iron in the melt, provided that the amount of manganese atoms arriving at the surface of the intermetallic compound per unit time is high enough to maintain the minimum manganese content of the phase necessary to keep the free energy below that of the Al_3Fe phase. (In a sample containing 1% iron and 0.2% manganese, solidified at a cooling rate of 100°C/min, this condition was not fulfilled, and the intermetallic phase found in that sample was of the Al_3Fe type).

It is a generally accepted opinion that iron suppresses the solid solubility of manganese. This is not so, but the growth mechanism proposed above furnishes a reasonable explanation of the observed effect.

At slow solidification rates, the intermetallic compound growing ahead of the α-dendrites develops in its most stable form, e.g. as $Al_6(Mn_{\frac{1}{2}}Fe_{\frac{1}{2}})$. That means that the iron concentration in the alloy ties an equal amount of manganese to the intermetallic phase. This reaction takes place just ahead of the growing α-phase. The manganese content in the liquid in contact with the solid α-phase is thereby decreased, and the concentration in the α-phase will therefore be lower than expected from the partition ratio for manganese and the original composition of the melt.

At higher rates of cooling, however, the low diffusion rate of manganese in the melt restricts the manganese content of the intermetallic phase. This leaves a higher concentration of manganese in the melt in contact with the growing α-phase, which therefore obtains a higher manganese content.

The fact that the growth of $Al_6(Mn,Fe)$ particles is restricted by the slow diffusion of manganese can be observed in microprobe scannings over the structure, where manganese concentration dips often are found just around the particles. This phenomenon will be discussed in the next section.

Some consequences of the formation of $Al_6(Mn,Fe)$ phase in other aluminium alloys

In commercial aluminium alloys the iron content is often between 0.2 and 0.5%. Manganese is often added to aluminium alloys in concentrations of 0.2–0.3%, mainly to increase the temperature of recrystallization. The capability of manganese in this respect is demonstrated in Fig. 59, where the temperature of beginning recrystallization, after 60% reduction in a cold rolling process, has been measured as a function of the manganese content.

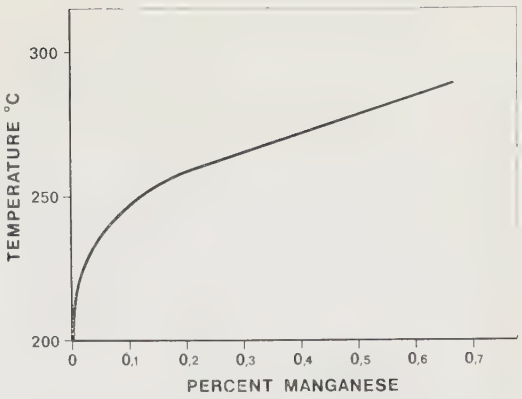

Fig. 59. Influence of manganese on the recrystallization temperature of aluminium after 60% reduction by cold rolling.

As a practical example, material of the AlZnMg type (5% Zn, 1.2% Mg, 0.3% Fe, 0.2% Mn and 0.2% Si) has been investigated at different rates of solidification. The behaviour described here is, however, the same in every aluminium alloy with a large freezing range.

In rapidly chilled material, the distribution of manganese is fairly even in the structure and fulfills its purpose of preventing the material from recrystallizing during the different steps of the production process.

When the cooling rates diminish, however, the mechanism discussed in the previous section will become more and more important. Iron will quickly be enriched ahead of the growing α-dendrites, and due to the presence of manganese the intermetallic phase $Al_6(Mn,Fe)$ forms, which of course has a high affinity for both iron and manganese in the remaining melt. The nucleation and start of growth of the manganese-iron intermetallic phase take place at a high temperature, when only a limited part of the total solidification process in this type of alloy has taken place. There is a considerable time available for the manganese-iron phases to grow before the temperature of the Al-Zn-Mg eutectic is reached at ≈475°C. During this long period of time these intermetallics will grow and absorb nearly all the iron and manganese available in the interdendritic areas of the material.

The microprobe line scanning over the structure

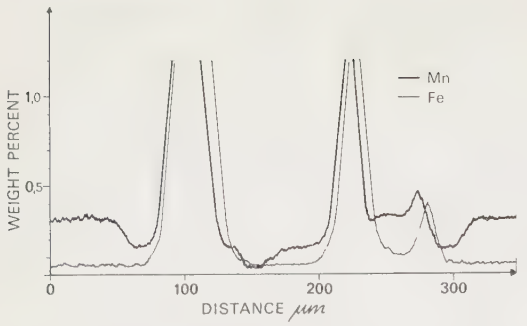

Fig. 60. Electron-microprobe line scanning showing the manganese and iron distribution in a slowly solidified ingot of an AlZnMg alloy.

of a slowly solidified sample of this alloy is shown in Fig. 60.

There is a very low manganese concentration to be found between the two $Al_6(Mn,Fe)$ particles shown.

When ingots of this material are processed, the recrystallization often starts in the depleted areas around $Al_6(Mn,Fe)$ particles. This is demonstrated in Fig. 61.

The number of grains in the recrystallized material will be a function of the number of large intermetallic crystals present in the ingot. In slowly cooled ingots, with a low number of $Al_6(Mn,Fe)$ particles, therefore, the recrystallized structure will be very coarse. The same mechanism also works (but in a less degree), in the normal aluminium-manganese alloys with 1% manganese and 0.5% iron.

The manganese content of zones depleted around each $Al_6(Mn,Fe)$ particle can be raised by diffusion of manganese from the α-phase.

Due to the slow diffusion rate of manganese in solid aluminium, however, this homogenization treatment has to take place at a high temperature (>600°C) and takes a considerable time. (The $Al_6(Mn,Fe)$ particles are stable enough not to dissolve or give away manganese to the depleted zone).

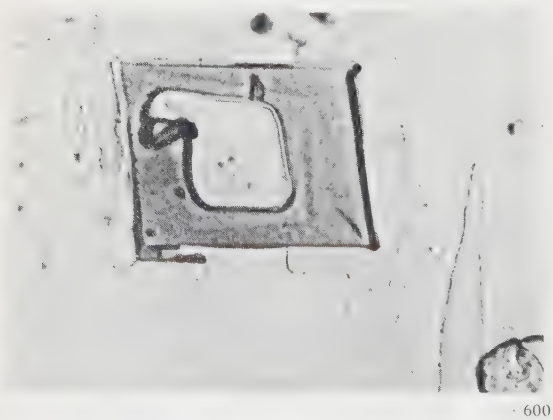

Fig. 61. Micrograph showing an $Al_6(Mn,Fe)$ particle in a slowly solidified ingot of an AlZnMg alloy. Recrystallization has just started in the manganese-depleted zone around the intermetallic crystal. Anodized. Polarized light.

Conclusions

It has been shown that in aluminium-manganese-iron alloys the kinetic factors, which control the mechanism of phase formation and growth, are as important as the composition, when the structure develops during the freezing process.

In alloys with ≈1% manganese an iron-rich $Al_6(Mn,Fe)$ phase nucleates and grows ahead of the α-dendrites. The heat-transfer rate controls the composition of the intermetallic phase and influences thereby the manganese content of the matrix.

In alloys with >2% manganese, the presence of iron considerably facilitates the nucleation and growth of the primary intermetallic $Al_6(Mn,Fe)$ phase, which in turn has an effect on the element and phase formation during the remainder of the solidification process.

High manganese concentration may be found in interdendritic areas of rapidly solidified material. In determining the properties of manganese-containing alloys, however, regions around primary intermetallics depleted in manganese seem to be more important.

There is often a necessity in technical processes to raise the manganese content of the depleted areas by an homogenization process rather than to even out relatively harmless regions of high manganese content.

The solubility of manganese in the α-phase is very little influenced by the presence of iron, but an increasing amount of manganese is tied to the intermetallic $Al_6(Mn,Fe)$ compound with decreasing cooling rate.

In a given casting process a high iron content of aluminium-manganese-iron alloys is beneficial (up to a limit where nucleation and growth of primary intermetallics can take place) in creating as many $Al_6(Mn,Fe)$ particles as possible, thereby decreasing the diffusion distances for manganese in the melt, and consequently decreasing the severity of manganese-depleted areas around these particles.

SUMMARY

Valuable information on nucleation and growth processes can be obtained by measurements of the dynamic undercooling at which solid phases grow from a melt. The dynamic undercooling contains a constitutional factor, which can be found from the phase diagram, and a kinetic factor, which depends on the rate of heat transfer, which in turn determines the growth rate.

Phase formation and growth mechanisms in the two very different systems aluminium-iron and aluminium-manganese have been investigated, and the structures developed have been discussed in relation to precise temperature measurements.

Among the results of interest in this work the following may be mentioned.

The conditions for formation of two different eutectic reactions in the aluminium-iron system have been clarified.

Due to the high dynamic undercooling at which the α-phase in aluminium-iron alloys grows, the iron content of the matrix is lower the higher the rate of cooling (within the limits of diffusion-controlled solidification).

In hyper-eutectic alloys of aluminium-iron as well as of aluminium-manganese it has been shown that the kinetic factors completely control the development of the structure.

The hyper-eutectic binary aluminium-manganese alloys are, due to the low constitutional factor, less influenced by the rate of heat transfer than the aluminium-iron alloys.

The dynamic factors control completely the structure development in aluminium-manganese-iron alloys.

A growth mechanism is proposed by which the element and phase distribution in the ternary alloys can be explained.

The intermetallic phase $Al_6(Mn,Fe)$ exists over the whole composition range from Al_6Mn to Al_6Fe.

In hyper-eutectic aluminium-manganese-iron alloys the phase can have any composition between Al_6Mn and $Al_6(Mn_{\frac{1}{2}}Fe_{\frac{1}{2}})$.

In hypo-eutectic aluminium-manganese-iron alloys the phase type exists only on the iron-rich side, e.g. from Al_6Fe to $Al_6(Mn_{\frac{1}{2}}Fe_{\frac{1}{2}})$.

A manganese-depleted zone is often formed around the $Al_6(Mn,Fe)$ particles.

ACKNOWLEDGEMENTS

I am grateful to AB Svenska Metallverken for supporting this work and for giving permission for its publication.

I also acknowledge my debt to my colleagues in the Central Research Laboratory of the Company for their invaluable practical assistance.

For the advice and encouragement given by Prof. G. Hägg, University of Uppsala, and Prof. R. Kiessling, Swedish Institute for Metals Research, Stockholm, I also express my sincere thanks.

I also wish to thank Prof. B. Chalmers, Harvard University, Cambridge Mass. USA, for his constructive advice and teaching in the field of solidification.

Finally, the facilities provided by The Swedish Research Councils' Laboratory, Studsvik, for making neutron-diffraction measurements, are gratefully acknowledged.

KINETISKA SYNPUNKTER PÅ BINÄRA OCH TERNÄRA LEGERINGSSYSTEMS STELNANDE

Sammanfattning

Värdefulla upplysningar om kärnbildnings- och tillväxtprocesser kan fås genom att bestämma den dynamiska underkylning vid vilken fasta faser tillväxer i en smälta. Den dynamiska underkylningen är sammansatt av en konstitutionell faktor, som kan erhållas ur tillståndsdiagrammet, och en kinetisk faktor, som beror av svalningshastigheten, vilken i sin tur bestämmer tillväxthastigheten.

Mekanismen för bildning och tillväxt av fast fas har undersökts i de båda sinsemellan mycket olika systemen aluminium-järn och aluminium-mangan, och de erhållna strukturerna diskuteras i relation till noggranna temperaturmätningar.

Av de erhållna resultaten kan följande särskilt nämnas:

Betingelserna för uppkomsten av två olika eutektiska reaktioner i aluminium-järn-systemet har klarlagts.

På grund av att tillväxten av α-fas i aluminium-järn-legeringar sker vid stor dynamisk underkylning blir grundmassans järnhalt lägre ju större svalningshastigheten är (inom gränserna för diffusionskontrollerat stelnande).

I övereutektiska aluminium-järn- och aluminium-mangan-legeringar bestäms strukturens utseende helt av den kinetiska faktorn.

På grund av den lägre fördelningsfaktorn påverkas aluminium-mangan-legeringarna mindre av svalningshastigheten än aluminium-järn-legeringarna.

De dynamiska faktorerna bestämmer helt strukturens utbildning i de ternära aluminium-mangan-järn-legeringarna.

En tillväxtmekanism föreslås genom vilken legeringselement- och fasfördelningen i de ternära legeringarna kan förklaras.

Den intermetalliska fasen $Al_6(Mn, Fe)$ har ett homogenitetsområde som sträcker sig från Al_6Mn till Al_6Fe.

I övereutektiska aluminium-mangan-järn-legeringar kan sammansättningen av denna fas variera mellan Al_6Mn och $Al_6(Mn_{\frac{1}{2}}Fe_{\frac{1}{2}})$.

I undereutektiska aluminium-mangan-järn-legeringar kan fasens sammansättning bara variera mellan Al_6Fe och $Al_6(Mn_{\frac{1}{2}}Fe_{\frac{1}{2}})$.

En på mangan utarmad zon bildas ofta runt de primära Al_6(Mn, Fe)-partiklarna.

REFERENCES

1. M. Hansen, Constitution of binary alloys. McGraw-Hill, New York 1958.
2. R. P. Elliott, Constitution of binary alloys. First supplement. McGraw-Hill, New York 1965.
3. D. Altenpohl, Aluminium und Aluminiumlegierungen. Springer-Verlag, Berlin 1965.
4. A. Roth, Die Löslichkeit von Eisen in Aluminium. *Z. Metallkunde 31 (1939) pp. 299–301.*
5. J. K. Edgar, Solubility of iron in solid aluminium. *Trans. Am. Inst. Min. Met. Engrs 180 (1949) pp. 225–229.*
6. C. Crussard & F. Aubertin, Etude thermoélectrique et thermodynamique d'alliages à base d'aluminium contenant Mg, Si, Fe ou Ti. *Rev. Métall. 46 (1949) pp. 661–675.*
7. G. V. Raynor & P. C. L. Pfeil, The constitution of the aluminium-rich aluminium-iron-nickel alloys. *J. Inst. Metals 73 (1947) pp. 397–419.*
8. A. J. Bradley & A. Taylor, X-ray study of the iron-nickel-aluminium ternary equilibrium diagram. *Proc. Roy. Soc. A 166 (1938) pp. 353–375.*
9. P. J. Black, The structure of $FeAl_3$. I. *Acta Cryst. 8 (1955) pp. 43–48.*
10. E. H. Hollingsworth, G. R. Frank, Jr & R. E. Willett, Identification of a new Al-Fe constituent, $FeAl_6$. *Trans. Am. Inst. Min. Met. Engrs 224 (1962) pp. 188–189.*
11. L. K. Walford, The structure of the intermetallic phase $FeAl_6$. *Acta Cryst. 18 (1965) pp. 287–291.*
12. B. Chalmers, Principles of solidification. John Wiley & Sons, New York 1964.
13. L. Bäckerud & B. Chalmers, Some aspects of dendritic growth in binary alloys. Part I. To be published.
14. J. W. Rutter & B. Chalmers, A prismatic substructure formed during solidification of metals. *Can. J. Phys. 31 (1953) pp. 15–39.*
15. W. A. Tiller, K. A. Jackson, J. W. Rutter & B. Chalmers, The redistribution of solute atoms during the solidification of metals. *Acta metallurg. 1 (1953)* pp. *428–437.*
16. L. Bäckerud, Some aspects of dendritic growth in binary alloys. Part II. To be published.
17. J. D. Hunt & K. A. Jackson, Binary eutectic solidification. *Trans. Am. Inst. Min. Met. Engrs 236 (1966) pp. 843–852.*
18. K. A. Jackson, Mechanism of growth. Liquid metals and solidification. *Am. Soc. Metals, Cleveland, Ohio 1958, pp. 174–186.*
19. R. Hultgren, R. L. Orr, P. D. Anderson & K. K. Kelley, Thermodynamic properties of metals and alloys. John Wiley & Sons, New York 1963.
20. J. C. Blade, J. W. H. Clare & H. J. Lamb, The recrystallization characteristics of dilute aluminium solid solutions prepared from zone-refined aluminium by levitation melting. *J. Inst. Metals 88 (1959–60) pp. 365–368.*
21. G. Trapied, Modified semi-continuous casting processes. *J. Inst. Metals 92 (1963–64) pp. 305–311.*
22. R. A. Oriani, Private communication.
23. G. Falkenhagen & W. Hofmann, Die Auswirkung extrem hoher Abkühlungsgeschwindigkeit auf die Erstarrung und das Gefüge binärer Legierungen. *Z. Metallkunde 43 (1952) pp. 69–81.*
24. H. D. Brody & M. C. Flemings, Solute redistribution in dendritic solidification. *Trans. Am. Inst. Min. Met. Engrs 236 (1966) pp. 615–624.*
25. H. Hanemann & A. Schrader, Ternäre Legierungen des Aluminiums. Verlag Stahleisen, Düsseldorf 1952.
26. D. Turnbull & B. Vonnegut, Nucleation catalysis. *Ind. Eng. Chem. 44 (1952) pp. 1292–1298.*
27. W. Hofmann, Röntgenographische Methoden in der Untersuchung von Aluminiumlegierungen. *Aluminium 20 (1938) pp. 865–872.*
28. A. D. I. Nicol, The structure of $MnAl_6$. *Acta Cryst. 6 (1953) pp. 285–293.*
29. M. A. Taylor, Intermetallic phases in the aluminium-manganese binary system. *Acta metallurg. 8 (1960) pp. 256–262.*
30. E. Degischer, Die Aluminiumecke im ternären System Aluminium-Eisen-Mangan. Aluminium-Arch. Band 18. Aluminium-Zentrale, Berlin 1939.
31. G. Phragmén, On the phases occurring in alloys of aluminium with copper, magnesium, manganese, iron, and silicon. *J. Inst. Metals 77 (1950) pp. 489–552.*
32. H. W. L. Phillips, The constitution of alloys of aluminium with manganese, silicon, and iron. I.—The binary system: aluminium-manganese. II.—The ternary systems: aluminium-manganese-silicon and aluminium-manganese-iron. *J. Inst. Metals 69* (1943) *pp. 275–316.*
33. G. V. Raynor, The effect on the compound $MnAl_6$ of iron, cobalt, and copper. *J. Inst. Metals 70 (1944) pp. 531–542.*
34. W. B. Pearson, Handbook of lattice spacings and structures of metals. Pergamon Press, London 1958.
35. H. W. L. Phillips, Annotated equilibrium diagrams of some aluminium alloy systems. Monograph 25, Institute of Metals, London 1959.
36. J. R. Lee, Liquidus solidus relations in the system iron-aluminium. *J. Iron Steel Inst. 194 (1960) pp. 222–224.*

ALMQVIST & WIKSELL 685298